UNIVERSITY OF GÄVLE

FACULTY OF ENGINEERING AND SUSTAINABLE DEVELOPMENT
Department of Building, Energy and Environmental Engineering

Analysis and simulation of shading effects on photovoltaic cells

Sara Gallardo Saavedra

June 2016

Student thesis, Master degree (one year), 15 HE

Energy Systems

Master Programme in Energy Systems

Course 2015/2016

Supervisor: Björn O Karlsson
Examiner: Nawzad Mardan

Abstract

The usage of conventional energy applications generates disproportionate emissions of greenhouse gases and the consumption of part of the energy resources available in the world. It has become an important problem which has serious effects on the climatic change. Therefore, it is crucial to reduce these emissions as much as possible. To be able to achieve this, renewable energy technologies must be used instead of conventional energy applications. Solar Photovoltaic (PV) technologies do not release greenhouse gas emissions directly and can save more than 30 million tonnes of carbon per exajoule of electricity generated relative to a natural gas turbine running at 45% efficiency.

Shadowing is one of the most important aspects that affects the performance of PV systems. Consequently, many investigations through this topic are being done in order to develop new technologies which mitigate the impact of shadowing during PV production. In order to minimise the impact of shadowing it is desired to be able to predict the performance of a system with PV-modules during shadowing.

In this thesis a simulation program for calculating the IV-curve for series connected PV-modules during partial shadowing has been developed and experimentally validated. PV systems modelling and simulation in LTspice environment has been presented and validated by means of a comparative analysis with the experimental results obtained in a set of tests performed in the laboratory of Gävle University. Experimental measurements were carried out in two groups. The first group corresponds with the experiments done in the string of six modules with bypass diodes while the measurements of the second group have been performed on a single PV module at HIG University.

The simulation results of both groups demonstrated a remarkable agreement with the experimental data, which means that the model designed at LTspice supposes a very useful tool that can be used to study the performance of PV systems. This tool contributes to the investigations in this topic and it aims to benefit future installations providing a better knowledge of the shading problem.

The master's thesis shows an in-depth description of the required method to design a PV cell, a PV module and a PV array using LTspice IV and the input parameters as well as the needed tests to adjust the models.

Moreover, it has been carried out a pedagogical study describing the effect that different shadow configurations have in the performance of solar cells. This study facilitates the understanding of the performance of PV modules under different shadowing effects.

Lastly, it has also been discussed the benefits of installing some newer technologies, like DC-DC optimizers or module inverters, to mitigate the shadowing effects. The main conclusion about this topic has been that although most of the times the output power will be increased with the use of optimizers sometimes the optimizer does not present any benefits.

Keywords: shading, PV model, LT-Spice, photovoltaic energy, bypass diode, DC-DC optimizer.

Acknowledge

Through these paragraphs I would like to express my gratitude for all the support that I have received during the execution of this master's thesis.

First of all, I would like to show my gratitude to my supervisor Björn Karlsson for all the knowledge that he has transmitted to me and his support during all these months.

Moreover, I would like to thank Mattias Gustafsson for helping me with the experimental measurements, for his advice and for his personal predisposition to support whenever he can.

Additionally, I would also like to thank Olle Olsson from Solarus for helping me with the instrumentation needed in the experimental measurements and to Joao Santos, also from Solarus, for showing his interest about my research and helping me whenever it has been possible.

Finally, I would like to express my gratitude to all the friends that I have met during this experience and to my family, partner and friends from Spain for their constant support. It would not have been possible without them.

Table of contents

Mater’s thesis: Analysis and simulation of shading effects on photovoltaic cells

List of figures

Mater’s thesis: Analysis and simulation of shading effects on photovoltaic cells

List of tables

Mater’s thesis: Analysis and simulation of shading effects on photovoltaic cells

1. Nomenclature

1M3P	Single Mechanism model, Three Parameters
1M4P	Single Mechanism model, Four Parameters
1M5P	Single Mechanism model, Five Parameters
A	Solar cell active area $[m^2]$
a-Si	Amorphous silicon
c-Si	Crystalline silicon cells
FF	Fill factor
G	Solar irradiance $\left[\frac{W}{m^2}\right]$
$I(V_{bias})$	Current in LTspice simulations to represent I-V curves [A]
I_{bypass}	Bypass current [A]
I_D	Diode current [A]
I_L	Light-generated current [A]
I_{mp}	Maximum power current [A]
I_{pv}	Illumination current associated to the photoelectric effect [A]
I_S	Reverse bias saturation current for the diode [A]
I_{SC}	Short-circuit current [A]
K_B	Boltzmann constant $\left[\frac{J}{K}\right]$
M(V)	Multiplication factor
MPP	Maximum Power Point
MPPT	Maximum Power Point Tracker
n	Diode ideality factor
NOCT	Nominal operation cell temperature [°C]
P_{in}	Power of the incident light [W]
P_{max}	Power in the MPP [W]

poly-Si	Polycrystalline silicon
PV	Photovoltaic
q	Modulus of the electron charge [C]
R_L	Load resistor [Ω]
R_S	Series resistor [Ω]
R_{Sh}	Parallel shunt resistor [Ω]
STC	Standard Test Conditions
T	Absolute temperature of the p-n junction [K]
V_{bias}	Voltage source in LTspice simulations to represent I-V curves [V]
V_{br}	Breakdown voltage [V]
$V_{irradiance}$	Voltage source in simulations to model the irradiance [V]
V_{mp}	Maximum power voltage [V]
V_{OC}	Open-circuit voltage [V]
α_{rel}	Short-circuit current temperature coefficient
β_{rel}	Open-circuit voltage temperature coefficient
ξ_{SQ}	Real performance index
η	Efficiency

2. Introduction

Nowadays, energy is a basic need all around the world. The use of energy is increasing enormously and therefore the population is starting to get concerned about the facts that this usage involves. The disproportionate emissions of greenhouse gases and the consumption of part of the energy resources available in the world have become important problems which have serious effects on the climatic change.

Therefore, it is crucial to reduce these emissions as much as possible. To be able to achieve this, renewable energy technologies must be used instead of conventional energy applications that use fossil fuels. Solar PV technologies do not release greenhouse gas emissions directly and can save more than 30 million tonnes of carbon per exajoule of electricity generated relative to a natural gas turbine running at 45% efficiency [1]. Additionally, PV systems have noiseless operations, are flexible in scale and have an easy maintenance in comparison with other renewable technologies.

The future perspectives of PV panels indicate that thin-film and other advanced technologies will dominate and be preferred in the future. Nevertheless, some investigations show that approximately 85%–90% of the actual PV market is still represented by single and multi-crystalline silicon cells (multi c-Si) [2]. The research that is been proposed for the master's thesis will study this silicon technology; specifically what effect the shadows have on its performance.

One of the most important problems which affects performance of PV systems is shadowing. In PV installations it is necessary to series connect a large number of solar cells to achieve sufficiently high voltage. When the cells are series connected the cell which delivers the lowest current will limit the current in the string. This means that a shadow on one cell will determine the performance of the whole circuit. The negative impact is partly minimized by connecting by pass diodes parallel to a number of cells. The diodes will conduct the current around the shadowed cell.

Many times, it is impossible to avoid or control the presence of shadows, which can appear due to many different reasons, for instance, objects near the system or clouds. For that reason, extensive research and development has been carried out. In order to minimize the impact of shadowing it is desired to be able to predict the performance of a system with PV-modules during shadowing. In this thesis a simulation program for calculating the IV-curve for series connected PV-modules during partial shadowing has been developed and experimentally validated.

2.1 Motivation

My personal interest in renewable energies is due to my environmental concern about global warming and air pollution. During the last few years, there have been many supportive programs from governments and other organizations which pursue the use of renewable energies. With my research, I would like to contribute to improve the knowledge of solar PV technology; its efficiency and reliability, to inspire its usage.

This thesis will contribute to the investigations in this topic and it aims to benefit future installations providing a better knowledge of the shading problem and a useful tool to evaluate its influence.

2.2 Objectives

This thesis aims to study the shading effect on the performance of solar PV modules.

The main objective is to design several electrical circuits which model a PV system in order to be able to simulate its performance when it is affected by different shadowing configurations. Furthermore, the thesis aims to verify the reliability of the designed models by means of comparing the simulation results with some experimental measurements carried out at the laboratory of the University of Gävle (at Hus 45 Heimdall).

In addition to this, other goal of this master's thesis is carrying out a theoretical and experimental study describing the effect that different shadow configurations have in the performance of solar cells and discussing the benefits of installing some newer technologies to mitigate the shadowing effects.

2.3 Thesis outline

The thesis begins with a theoretical review of all the important points needed to carry out and understand the analysis that are shown throughout the thesis. It starts with a brief explanation of the PV energy. Secondly, the different ways of modelling a solar cell are summarised. After that, in order to understand the I-V curves that will be analysed in the results, these curves have been plotted and also the effect that irradiance and temperature have on them. To finish the introduction, there is a review of the shadowing problems; also of the existing technology to mitigate their effects and the possible damages due to shadows cast across solar cells.

In the following section, the method used to perform the LTspice simulations and the experimental measurements at HIG laboratory have been explained.

Later on, all the results and charts obtained from the simulations and tests are shown and discussed.

As a final point, the most important conclusions of this master's thesis are summarised.

2.4 Limitations and delimitations

Although models play an important role they have also limitations. The models designed will try to conform to reality as much as possible; nevertheless it will be necessary to perform some real experiments to prove the consistency of the results obtained with the simulations. To validate one PV module model will be necessary to perform at least one experimental measurement to adjust some values and to verify its correct operation.

Some chosen delimitations have to be mentioned. The simulations will be carried out using LTspice software, although there are alternative programmes that could be used. Additionally, the devices studied will be the ones that are in the HIG laboratory; bypass diode, DC-DC optimizer and module inverter.

3. Theory

3.1 Photovoltaic energy

3.1.1 Basics

A photovoltaic cell is an electrical device that converts the energy of light into electricity. The photovoltaic effect is a physical and chemical phenomenon. It has suitable metal contacts, usually on the top and bottom, which collect the minority carriers crossing the junction under irradiation and serve as the output terminals [3]. Photovoltaic modules and arrays produce DC electricity. Figure 1 represents the components of a solar cell.

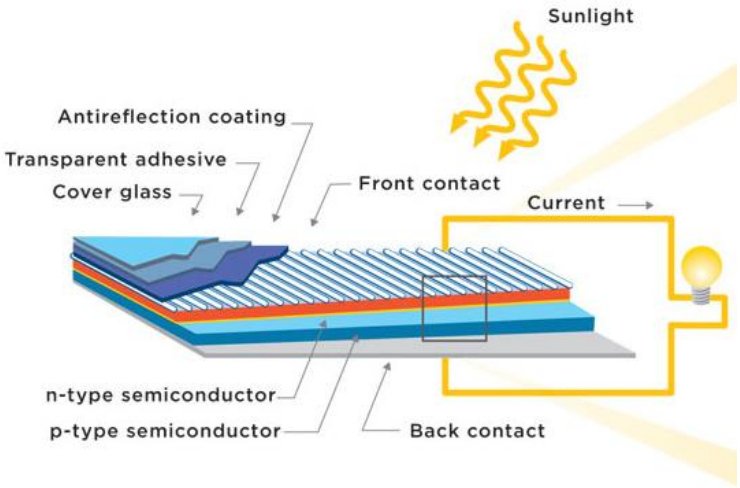

Figure 1: Solar cell composition [4]

The output of an individual cell is rather low. A photovoltaic module is a number of solar cells electrically connected to each other and mounted in a structure. A set of modules connected together form an array. The modules can be connected in both series and parallel to produce any required voltage and current combination, forming a PV array. All these connections are represented in Figure 2.

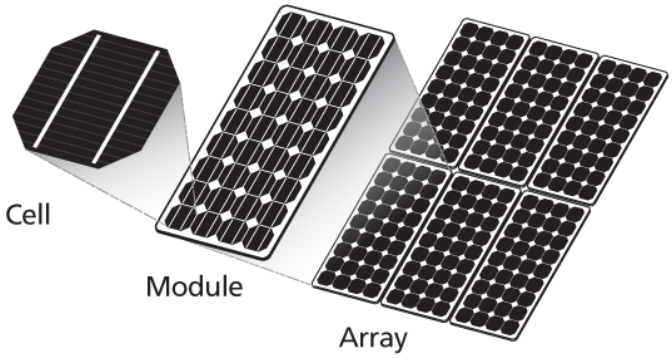

Figure 2: PV cell, module and array [5]

3.1.2 Semiconductor materials

The materials used to manufacture the solar cells are called semiconductor materials. They work as conductors when energy is available and as insulators in other cases. Nowadays, most solar cells are made by silicon-based, since this is the most mature technology. However, other materials are under active investigation and may supersede silicon in the long term [6]. This master's thesis will be focused in silicon-based cells.

There are three mainly types of semiconductor materials used for solar cells; crystalline, multicrystalline and amorphous semiconductors.

- In crystalline silicon (c-Si) the atoms are arranged in a regular pattern and consequently it is the most expensive type of semiconductor material.

- The multicrystalline or polycrystalline silicon (poly-Si) is composed by regions of crystalline Si separated by 'grain boundaries', where bounding is irregular.

- In the amorphous silicon (a-Si) there is no order in the structural arrangement of the atoms, resulting in areas within the material containing unsatisfied bonds.

The PV technology is progressing continuously. Because of the cost, performance and fabrication points of view, the application of new advanced materials has created new generations of solar cells [7].

3.2 Modelling of a solar cell

Numerous models have been made in order to simulate the performance of solar cells. The numerical method used to model the electrical behaviour, the load current and load voltage of a solar photovoltaic cell or panel, is based on the use of the equivalent circuit for a photodiode. Equivalent circuit models define the entire I-V curve of a cell, module, or array as a continuous function for a given combination of operating conditions. The *single-diode* model and the *two-diode* model are the most commonly used.

3.2.1 Single-diode model

The *single-diode* model is widely used and it has results generally acceptable [8]. Three equivalent circuit models can be used to describe a *single-diode* model [9].

The first of all is the ideal solar cell, represented in Figure 3, also called 1M3P model (Single Mechanism, Three Parameters). For an ideal model, a solar cell can be simply modelled by a p-n junction in parallel with a current source that is associated to the photo carriers generated. The three parameters are the illumination current associated to the photoelectric effect I_{pv}, the reverse bias saturation current for the diode I_S and n, the diode ideality factor.

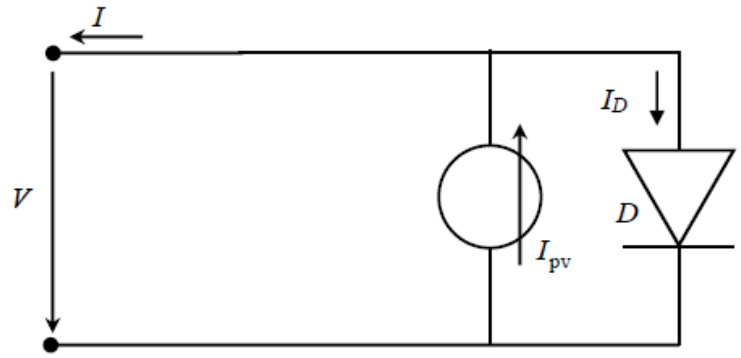

Figure 3: Ideal *single-diode* model of a solar cell [8]

The equations for this model are:

$$I = I_{pv} - I_D \tag{1}$$

$$I_D = I_S\left(e^{\frac{q\,V}{n\,K_B T}} - 1\right) \tag{2}$$

In the equations (1) and (2), K_B is the Boltzmann constant (1.38062E-23 $m^2 kg\ s^2 K^{-1}$), q is the modulus of the electron charge (1.602E-19 C), T is the absolute temperature of the p-n junction and V is the output voltage. The illumination current associated to the photoelectric effect is proportional to the solar irradiance G and to the solar cell active area A.

More accuracy can be introduced to the model by adding a series resistance, Figure 4. The solar cell with series resistance, commonly known as 1M4P model (Single Mechanism, Four Parameters), takes into account the influence of contacts by means of a series resistance R_S. The unknown parameters of this model are: I_{pv}, I_S, n and R_S.

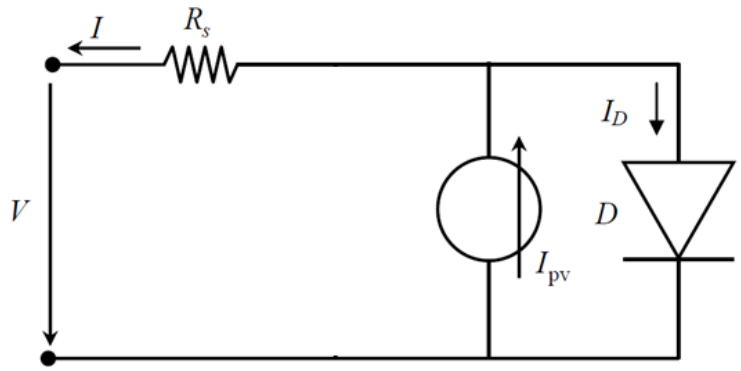

Figure 4: S*ingle-diode* model 1M4P of a solar cell [8]

In this model the equation (1) is still working while the new diode current expression is introduced in the equation (3).

$$I_D = I_S\left(e^{\frac{q\,(V+IR_S)}{n\,K_B T}} - 1\right) \tag{3}$$

These models are not accurate enough, as they do not take into account some real factors in the solar cells. For that, it is necessary to introduce one more precise and

realistic solar cell model. It is the solar cell with series and shunt resistances, 1M5P model (Single Mechanism, Five Parameters), shown in Figure 5. The R_{Sh} parallel shunt resistor takes into account the leakage currents. The five parameters of this model are: I_{pv}, I_S, n, R_S and R_{Sh}.

In this case, the current equation can be deduced directly by using the Kirchhoff law and it is given by the equations (4) and (5).

$$I = I_{pv} - I_D - I_{Sh} \tag{4}$$

$$I = I_{pv} - I_S\left(e^{\frac{q\,(V+I\,R_S)}{n\,K_B T}} - 1\right) - \frac{V + I\,R_S}{R_{Sh}} \tag{5}$$

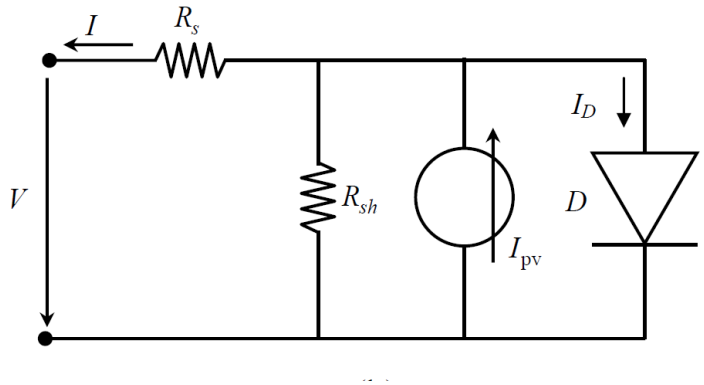

Figure 5: Real *single-diode* model of a solar cell [8]

When there is an increment in the shadow rate the series resistance increases. In contrast, the shunt resistance presents a clear reduction due to shading [10]. It means that when the shadow rate increases, the leakage current and the voltage drop in the contacts will be higher. The probabilities of hot spot apparition increase when the R_{Sh} decreases its value, as it is working as a load in reverse bias. It has been proven that the major contribution to the reduction of output power as a result of shading is due to series resistance, as the power dissipated by R_S can be 50%, or even more, of the total power reduction at the PV module output [10].

3.2.2 Two-diode model

This model takes into account the generation and recombination rates in the transition region of a p-n diode by introducing another diode in parallel, which may be significant under some thermal or illumination conditions in high band gap semiconductor.

At lower values of irradiance and low temperatures, *two-diode* model (Figure 6) gives more accurate curve characteristics than the *single-diode* model. Nevertheless, the number of equations and unknown parameters increases to two, making calculations more complex, as now there will be two unknown diode quality factors.

The *two-diode* model can be solved by equations (6) and (7) [12].

$$I = I_{pv} - I_{D1} - I_{D2} - I_{Sh} \tag{6}$$

$$I = I_{pv} - I_{S1}\left(e^{\frac{q\,(V+I\,R_S)}{n1\,K_B T}} - 1\right) - I_{S2}\left(e^{\frac{q\,(V+I\,R_S)}{n2\,K_B T}} - 1\right) - \frac{V + I\,R_S}{R_{Sh}} \qquad (7)$$

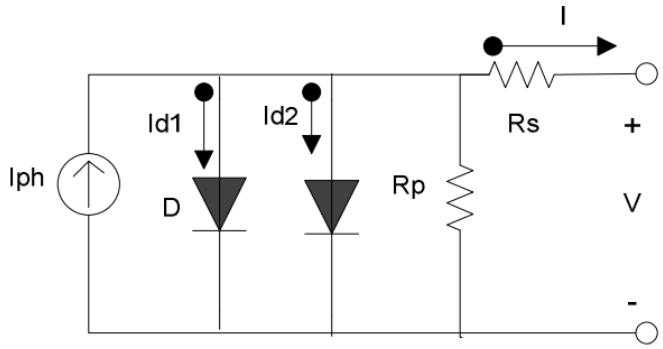

Figure 6: *Two-diode* model of a solar cell [11]

In equation (7), n1, n2 and I_{S1}, I_{S2} correspond to the ideality factor and the saturation current of the first and second diodes respectively and R_{Sh} is represented by R_p in Figure 6. The diodes voltage can be expressed as $(V + I * R_S)$.

So taking all aspects into consideration, it will be use the single diode model, as it is faster due to less complex equation and also the computational errors are less. This model will be not considered in the present work.

3.2.3 Reverse bias models

The models explained above have been reviewed to deal with the hot spot singularities and with the reverse characteristics, when solar cells are working in reverse bias. One of the first approaches modifies the one diode model with the assumption that the avalanche multiplication affects mainly the direct current, introducing the multiplication factor M(V), which denotes the effect of the avalanche effect. This model can be seen in Figure 7.

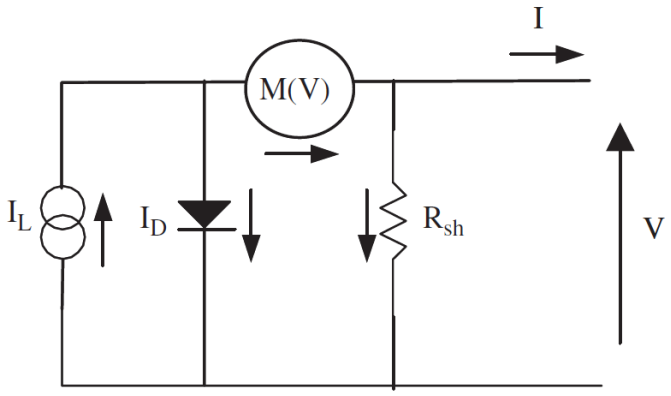

Figure 7: Reverse bias electrical model considering the avalanche effect [13]

Bishop proposes an equation where the avalanche effect is expressed as a non-linear multiplication factor that affects the shunt resistance current term. Bishop's model (Figure 8) has been used in most of the works to study the mismatch effects in solar

cell interconnection to form PV modules [10]. These two models will be not considered in the present work.

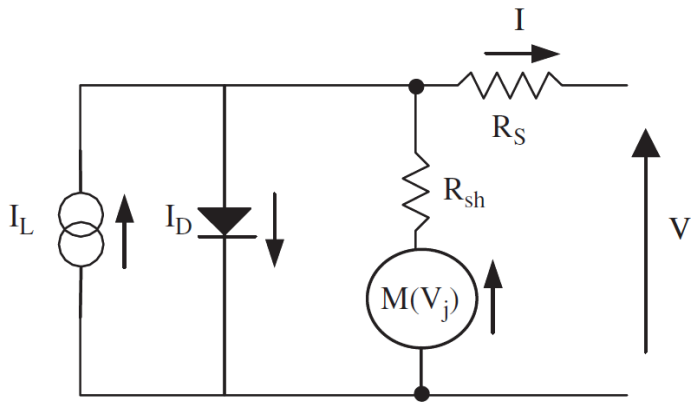

Figure 8: Bishop's reverse bias electrical model [13]

3.3 I-V curve plotting

The I-V curve of a PV string delineates its energy conversion capability at the existing conditions of irradiance and temperature. The curve represents the combinations of current and voltage at which the string could be operated or loaded, if the irradiance and cell temperature could be held constant.

In the Figure 9 it is showed typical I-V and P-V curves and the key points on these curves. The P-V curve is calculated from the measured I-V curve.

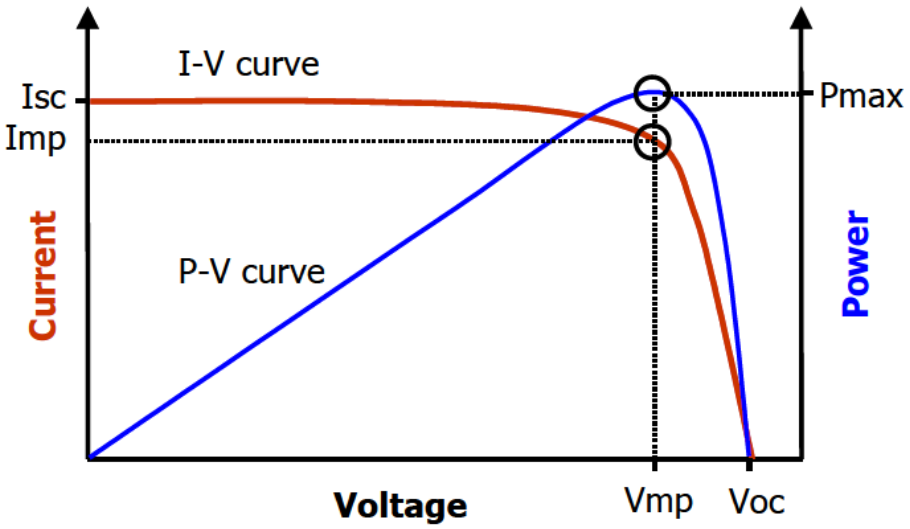

Figure 9: The I-V and P-V curves of a photovoltaic device [14]

The current through the solar cell when the voltage across it is zero is known as short-circuit current I_{SC} (at short circuit current condition; load $R_L = 0\ \Omega$).It can be obtained from equation (5) when V=0V:

$$I_{SC} = I_{pv} - I_S\left(e^{\frac{q\,I_{SC}\,R_S}{n\,K_B T}} - 1\right) - \frac{I_{SC}R_S}{R_{Sh}} \qquad (8)$$

I_{SC} is due to the generation and collection of light-generated carriers. The short circuit current and the light generated current, I_L or I_{pv}, can be considered identical in an ideal solar cell [15]. Therefore, the short circuit current is the largest current which may be obtained from the solar cell.

The open-circuit voltage V_{OC}, is the maximum voltage available from a solar cell, and it occurs at zero current. It corresponds to the amount of forward bias on the solar cell due to the bias of the solar cell junction with the light-generated current. Its value can be obtained from equation (5) when I=0A, as it is expressed in (9).

$$V_{OC} = \frac{nK_BT}{q} * \ln\left(\frac{I_{pv}}{I_S} + 1\right) \tag{9}$$

The saturation current I_S depends on recombination in the solar cell. V_{OC} is then a measure of the amount of recombination in the device. I_S can be calculated using equation (9) when the rest of parameters are known (10).

$$I_S = \frac{I_{SC} - \frac{U_{oc}}{R_p}}{\left(e^{\frac{q*U_{OC}}{nkT}} - 1\right)} \tag{10}$$

The Maximum Power Point, MPP (I_{mp}, V_{mp}),is the point at which the array generates maximum electrical power, which means that the product of current and voltage reaches the maximum value of the curve. It is located at the “knee” of the curve.

According to the power convention, the power related with the diode is Pcell=-VI. In the PV quadrant of the stationary current-voltage characteristic this value is negative, meaning that in this zone the device is active or, equivalently, the power is delivered by the solar cell and given by (11):

$$P = -P_{cell} = V\left(I_{pv} - I_S\left(e^{\frac{q\,(V+IR_S)}{n\,K_BT}} - 1\right) - \frac{V + IR_S}{R_{Sh}}\right) \tag{11}$$

It can be introduced the index ξ_{SQ} [16] to calculate how far a real solar cell is from its ideal performance. It takes into account that the efficiency will decrease due to limiting effects, such as series resistance losses, non-radiative recombination or overheating. This index can be calculated as the rate of the real and the ideal efficiencies. In the literature, researchers talk about the fill factor (FF) which provides an easy comparison for the performance of a cell compared to the theoretical maximum. FF is the ratio of two areas defined by the I-V curve, as it can be seen in Figure 10. Although physically unrealizable, an ideal PV module technology would produce a perfectly rectangular I-V curve in which the maximum power point coincided with (I_{SC}, V_{OC}), for a fill factor of 1.

Therefore, FF can be calculated by (12):

$$FF = \frac{I_{mp}V_{mp}}{I_{SC}V_{OC}} \tag{12}$$

The actual magnitude of the fill factor depends strongly on module technology and design. For example, amorphous silicon modules generally have lower fill factors than crystalline silicon modules [14].

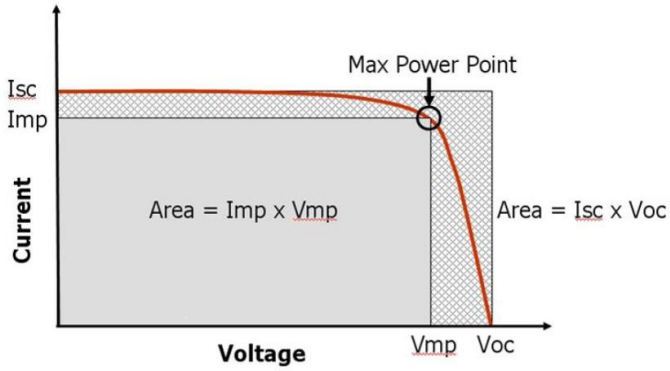

Figure 10: Fill factor, defined as the grey area divided by the cross-hatched area [14]

Any factor that reduces FF also reduces the output power by reducing I_{mp}, V_{mp} or both. The I-V curve itself helps us identify the nature of these impairments. The effects of series losses, shunt losses and mismatch losses on the I-V curve are represented in Figure 11.

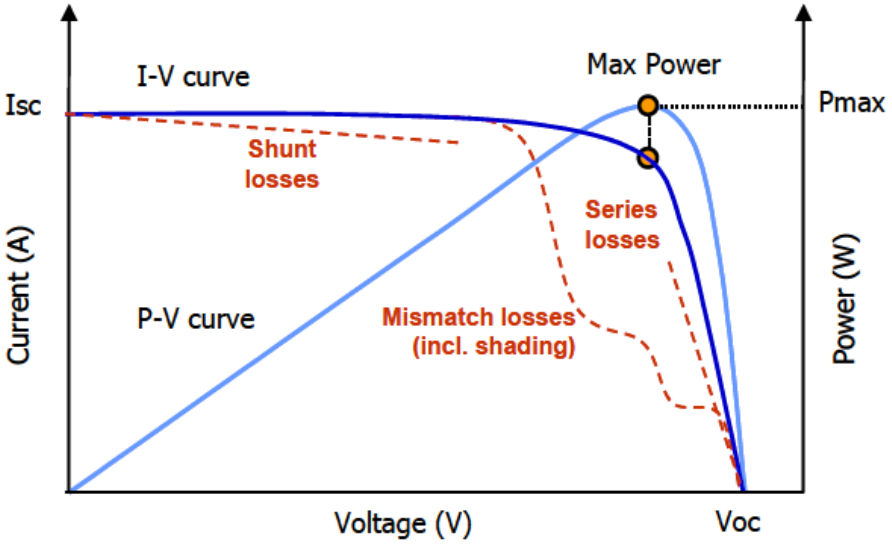

Figure 11: Several categories of losses that can reduce PV array output [14]

Only part of the solar radiation incident on the solar cell is converted to electricity. The ratio of the output electrical energy to the input solar radiation is defined as the efficiency value η (13) and it depends on the type of cell. The efficiency of a PV module is lower than the one of a solar cell, as not all the area of the module is covered by cells [17].

$$\eta = \frac{FF\ I_{SC}V_{OC}}{P_{in}} = \frac{I_{mp}V_{mp}}{P_{in}} \tag{13}$$

Where P_{in} is the power of the incident light, product of the incident light irradiance, measured in $\frac{W}{m^2}$at the surface area of the solar module (m^2).

3.4 Effect of irradiance and temperature

The light intensity or irradiance has a dominant effect on current parameters. The short circuit current and the maximum current increase linearly with increasing light intensity. This can be observed in Figure 12. Therefore, concentrating systems such as Fresnel lenses and Booster mirrors can be used to increment photocurrent, short circuit current and maximum current values of module. The cell temperature slightly affects the short circuit current, increasing it a bit with the temperature increment. All these effects can be calculated by (14):

$$(I_{SC})_{G,T} = (I_{SC})_{STC} * \left(1 + \alpha_{rel} * (T - T_{STC})\right) * \frac{(G)_{G,T}}{G_{STC}} \quad (14)$$

Where STC denotes the Standard Test Conditions ($T_{STC} = 25°C$ and $G_{STC} = 1000\,\frac{W}{m^2}$) and α_{rel} is the relative current temperature coefficient.

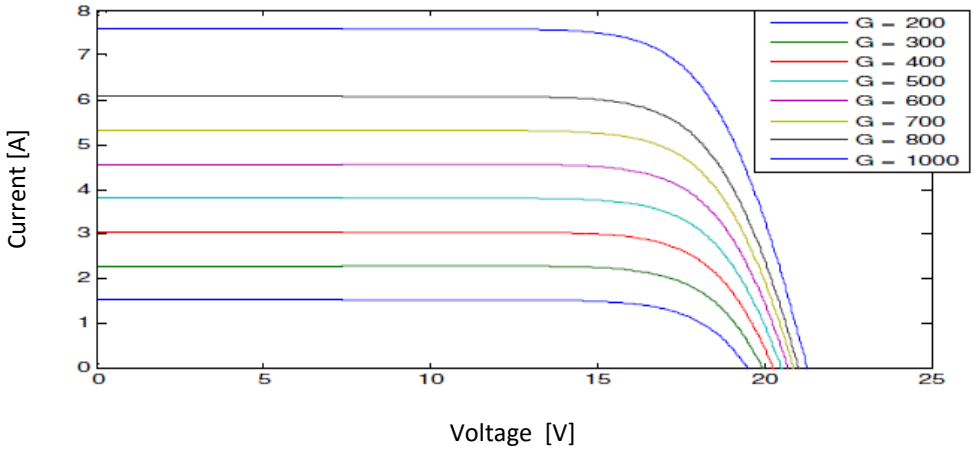

Figure 12: I-V characteristics of single diode for varying irradiance G[W/m2] [18]

It has been found that the series resistance decreases with increasing light intensity due to the increase in conductivity of the active layer with the increase in the light intensity. On the other hand, parallel resistance also decreases with light intensity. This decrement can be explained in terms of a combination of tunnelling and trapping of the carriers through the defect states in the space charge region of the device [18]. Figure 13 shows this tendency.

Otherwise, it has been observed that module temperature has a high effect on voltage parameters. Open circuit voltage and maximum voltage decrease with increasing module temperature, following equation (15). Figure 14 shows this tendency.

$$(V_{oc})_T = (V_{oc})_{STC} * \left(1 + \beta_{rel} * (T - T_{STC})\right) \quad (15)$$

It has been found that the series resistance of mono-crystalline modules have a small increase when temperature increases, while the poly-crystalline modules show a small

decrease with temperature. On the other hand, it has been found that the parallel resistance of mono-crystalline modules decrease with temperature. The parallel resistance of poly-crystalline module increase with temperature [18].

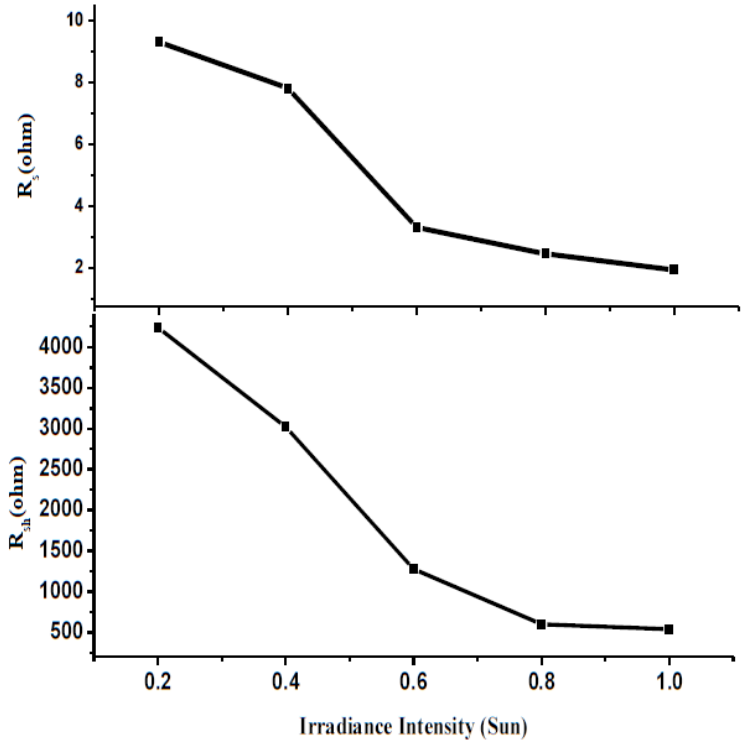

Figure 13: Light intensity dependency of series and parallel resistances on mono-crystalline silicon (mono c-Si) [18]

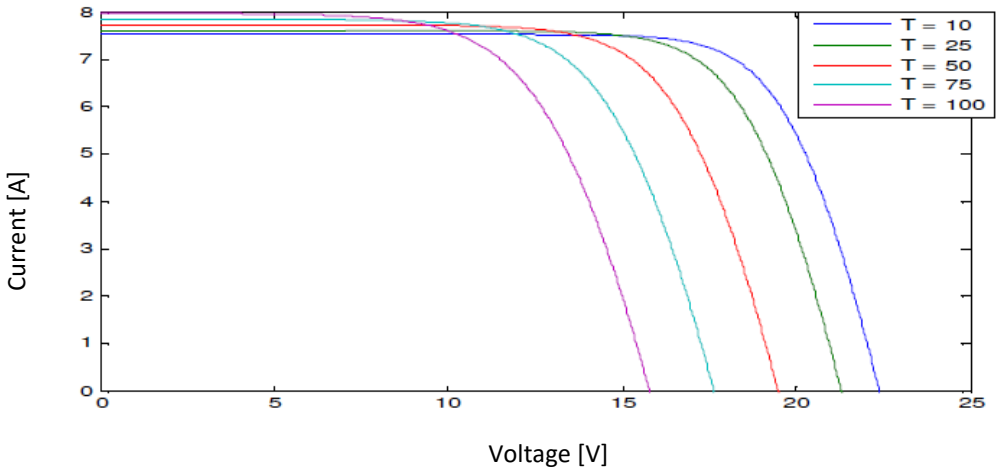

Figure 14: I-V characteristics of single diode for varying temperature T [C] [18]

The best way to improve the performance of solar system is maximizing the light intensity falling on the PV module and also to avoid the drop in V_{OC} and V_{mp} keeping the module temperature as low as possible [18].

3.5 Shading of solar cells

Since the maximum voltage given by a solar cell is approximately 0.65V, cells are connected in series in order to collect higher voltage or in parallel to generate higher current, forming PV modules with the desired output. When one of the cells is partially shadowed, it will produce less current than the rest of the cells in the string, as the photo-current goes in the reverse direction. The other cells will try to push more current through the poor cell than it delivers. This is however not possible, since in this case the cell acts as a diode in the reverse direction. Then the current of this cell will limit the current of the whole string [16]. The conventional solution to mitigate shading problem are the bypass diodes. There are some newer solutions for minimizing the impact of shading, as DC-DC optimizers or module inverters [19]. As a result of shading, multiple local MPP appear in the power curve, Figure 15.

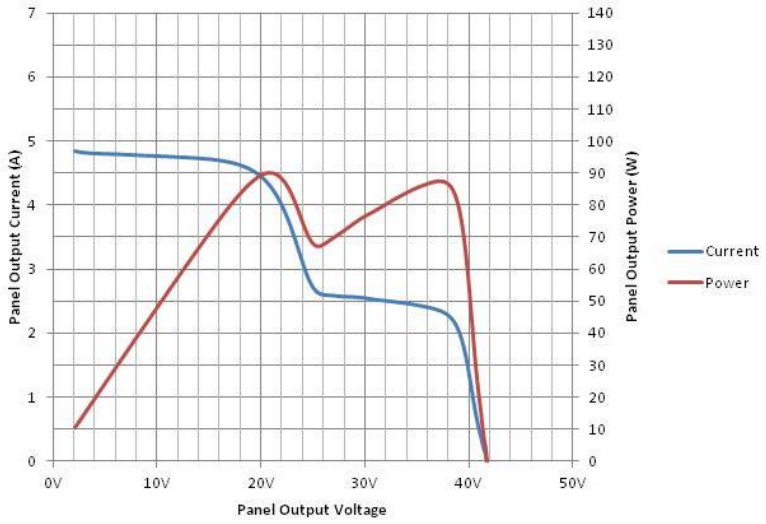

Figure 15: I-V and P-V curves with multiples local MPP due to shading

Therefore, to obtain the global MPP, a Maximum Power Point Tracker (MPPT) which can track the global power point is necessary. The DC-DC optimizers and module inverters usually incorporate this function.

3.5.1 Bypass diode

In order to avoid the shading problem, the conventional solution is to install bypass diodes. A bypass diode is connected in parallel, but with opposite polarity. Under normal operation, each solar cell will be forward biased and therefore the bypass diode will be reverse biased and will be an open circuit which will not conduct. However, if a solar cell is reverse biased due to a mismatch in short-circuit current between several series connected cells as a consequence of shading, for instance, then the bypass diode conducts, thus allowing part of the current from the unshaded solar cells to flow in the external circuit. Figure 16 shows five bypass diodes connected in parallel with five cells in series connected.

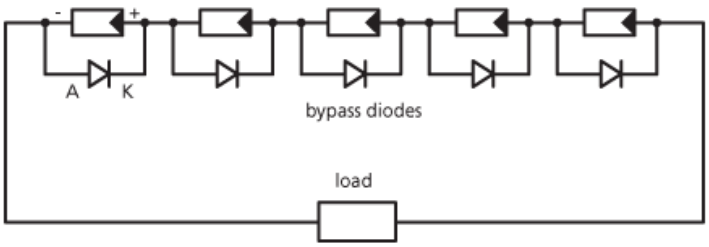

Figure 16: Bypass diodes installed in five solar cells [5]

In practice, one bypass diode per solar cell is generally too expensive and instead bypass diodes are usually placed across groups of solar cells. Generally, for a solar cell string of n cells being equipped with one bypass diode, the absolute value of the breakdown voltage, V_{br}, of a reverse biased solar cell must be greater than n up to n+1 times 0.5V. This value is the equivalent to the voltage in the MPP of the rest of the cells in series which are not shadowed (n-1) plus the voltage of a silicon bypass diode that is usually between 0.5 and 1V [20]. Figure 17 illustrates a string of n cells connected with a bypass diode through which is circulating a current I_{bypass}. Considering that the voltage increment in each cell and the voltage drop in the bypass diode is 0.5V, the shadowed cell has the following voltage drop (16):

$$\Delta V = (n-1)0.5 - (-0.5)\ V = 0.5n\ V \tag{16}$$

Because of that fact, V_{br} of a reverse biased solar cell must be greater than n up to n+1 times 0.5 V, not to achieve the breakdown value which will generate serious damages in the cell.

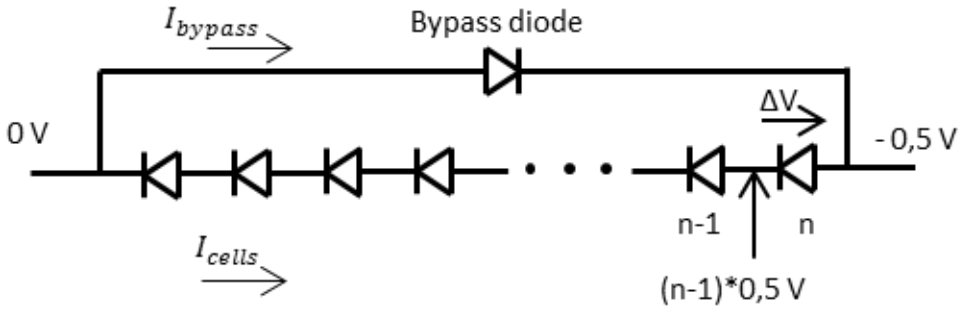

Figure 17: Current through bypass diode when a cell is shaded

If the V_{br} is higher than this value, the current will be lower than the maximum that the un-shadowed cells can generate and the power output will probably be lower than the maximum. Actual crystalline silicon solar cells have lower V_{br} than -10 V [21]. Therefore, one bypass diode is applied typically per each 18 cells in series. As a consequence, larger voltage differences cannot arise in the reverse current direction of the solar cells.

3.5.2 DC-DC Optimizer

DC-DC optimizers are devices which convert a current from one voltage level to another in order to mitigate the effect of PV modules shading. The power of this source has to be constant, thus voltage for current multiplication is not allow to change.

If each module has each own DC-DC optimizer and these optimizers are connected in series, Figure 18, the current of all of them have to be the same. Therefore, if one module is shadowed and is generating less current than the others, the DC-DC optimizer would have to increment its current at the expense of reducing its voltage. Therefore, the current of this module will not limit the current of the whole system.

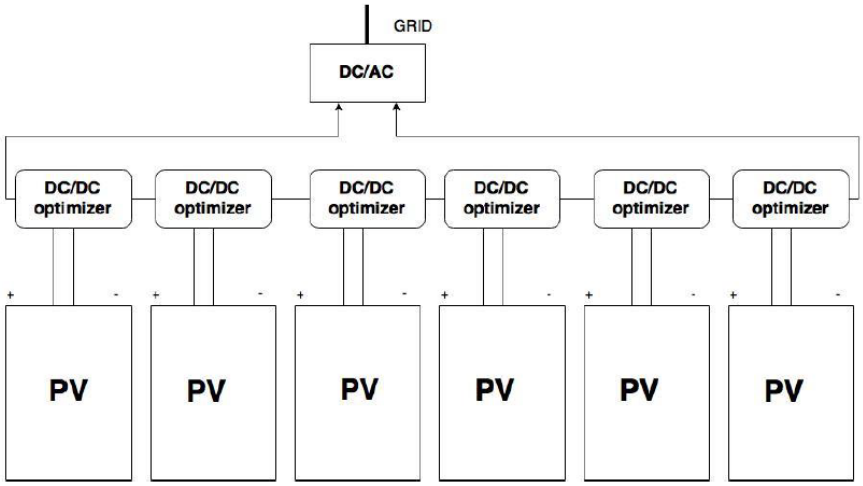

Figure 18: TIGO DC-DC Optimizer system installed at HIG University laboratory [19]

In Figure 19 can be seen the DC-DC optimizers installed in a PV System in the laboratory of the University of Gävle.

Figure 19: PV system with DC-DC optimizer [19]

3.5.3 Module inverter

On the other hand, the inverter is a device which converts from DC current to AC current. As solar panels produce DC current this device is necessary to connect the current generated with the panels to the grid. One solution to minimize the impact of shading is by using module inverters instead of string inverters.

String inverters are the traditional inverters used in PV solar applications. In this case, the modules are linked in series and an inverter is connected to the string to convert to AC current, as it is showed in Figure 20.

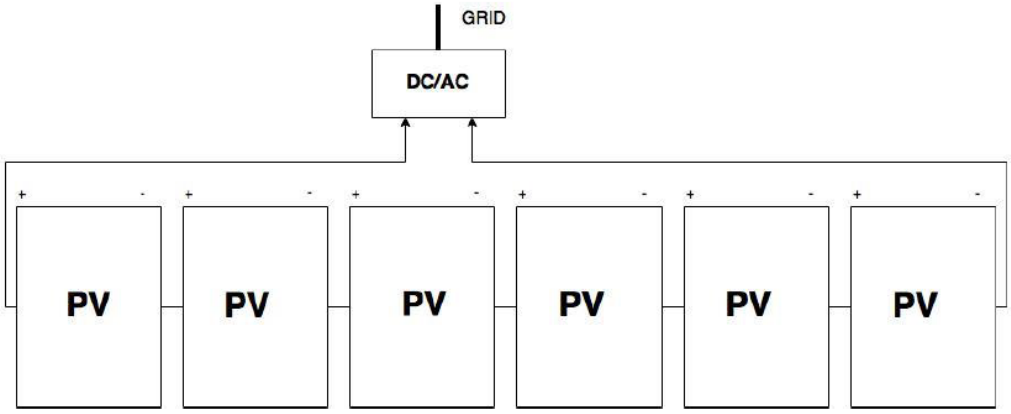

Figure 20: String inverter system [19]

This is the perfect solution in absence of shading, as the voltage of the string is greater than the one of an individual module and so the conversion is easier and the costs of the inverters are minimized. However, when there is shading all the panels will not generate the same current and using a module inverter (micro-inverter) has the advantage that the shadowed modules does not affect the other modules, as the DC current of each module is directly convert in each module inverter to AC current. In Figure 21 is represented a schematic of six PV modules with three module inverters. In this case, each micro-inverter can convert the DC current from two different panels.

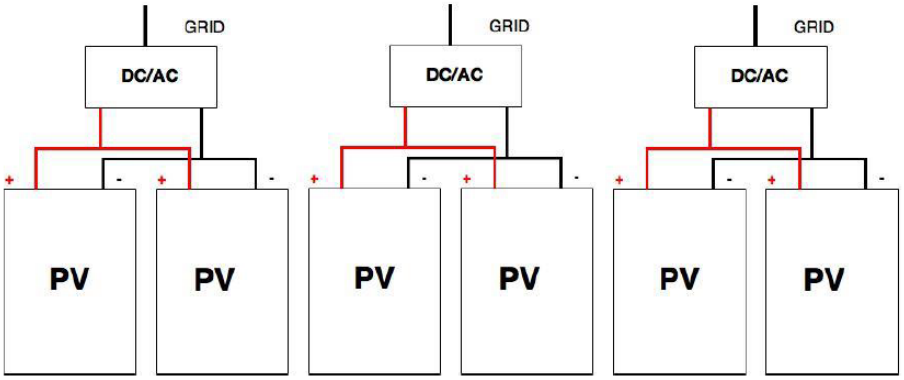

Figure 21: PV system using module inverters [19]

3.5.4 System components and prices

The components of each of the three systems explained above and their price are summarised in Table 1 [19].

The most expensive system of the three studied is the DC-DC optimizer, followed by the module inverter.

Table 1: Components and prices of the three systems at HIG laboratory

System	Components	Price [SEK]
String inverter (bypass diodes)	6 PV modules + 1 Inverter	18330
DC-DC Optimizer TIGO	6 PV modules+3 Maximizers + 1 MMU + 1 Tigo Energy Gateway + 1 Inverter	27446
Module inverters	3 Micro Inverters+ 6 PV Modules	21000

3.6 Damages in solar cells due to shading

As it has been explained above, if a PV module is partially shaded, some of its cells can work in reverse bias, working as loads and not as power generators (consuming instead of generating power) [10]. This happens because when a solar cell is shadowed the current photo generated by the illuminated solar cells is forced through the shadowed solar cell that will become reverse biased. If the shadowed solar cell has a sufficiently high R_{sh} the entire system is turned off since the current generated by the illuminated solar cells cannot flow through the shadowed one. On the contrary, if the R_{sh} of the shadowed solar cell is sufficiently low, it acts as a load and the cell can dissipate tens of watts [22]. If the saturation current of silicon diode I_S increases, the reverse current increases [23]. These two parameters determine the solar cell type. In the Figure 22 it can be seen a reverse bias model of a solar cell.

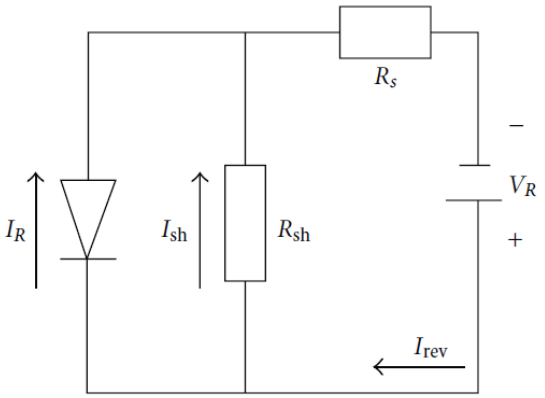

Figure 22: Reverse bias model [23]

When reverse bias exceeds the V_{br} value of the shaded solar cell, the cell will be fully damaged. It can appear, for example, cell cracking or hot spot formation (Figure 23) and therefore an open circuit occurs at the serial array where the cell is connected. The breakdown patterns consist on many microscopic breakdown spots through which a local leakage current flow. A hot spot can be formed in case of the leakage is very large, which would destroy the module.

Figure 23: Hot spot phenomena [23]

In order to avoid this problem, the use of many bypass diodes ensures the reduction of the thermal effects, to prevent the ageing of PV cells and maintain good values of produced power. The R_{sh} value is highly dependent on the quality of the solar cell production process. In particular silicon impurities and poor edge isolation are the main causes of shunt paths formation [22].

4. Method and process

After having done an in depth review of the background theory required to understand the carried out research, in these paragraphs it will be explained the method applied to obtain the results and conclusions of this master's thesis. The first section explains the LTspice models, the second shows the instruments used at HIG University to carry out the measurements and finally, the third section describes the cases that will be studied.

4.1 LTspice IV simulations

4.1.1 LTspice IV

The software used to model and implement the simulation has been LTspice IV, which is a free computer programme, produced by the semiconductor manufacturer Linear Technology (LTC). The program logotype is introduced in Figure 24. It implements a Spice simulator of electronic circuits. It can be downloaded at their website [24].

Figure 24: LTspice logotype

4.1.2 Solar cell modelled with LTspice IV

As it has been explained in the theory, the model selected to do the simulations is the real *single-diode* model of a solar cell (1M5P). First of all, it has been designed the model of a solar cell which later on has been used to create the desired PV module and PV array. The solar cell created in LTspice can be seen in Figure 25.

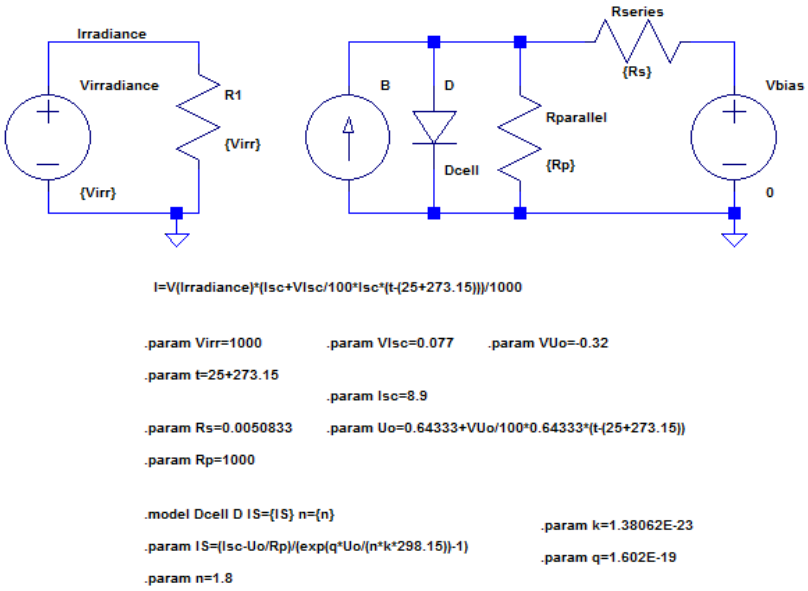

Figure 25: Real *single-diode* model of a solar cell designed in LTspice IV

The different electrical components used and its parameters are going to be introduced below.

- Firstly, it has been added a voltage source in parallel with a resistance. The volts and ohms value are the same (Virr equal to 1000 V and 1000 Ω in the case of Figure 25) so that the current through this circuit is 1 A. Therefore the irradiance value, which can be calculated multiplying the voltage by the current, has the same value as the voltage source ($G = V_{irradiance}$). Changing this value, it can be controlled the irradiance.

- Secondly, a DC current source that depends on the irradiance and temperature level, using equation (14) of the theory.

- Thirdly, the open circuit voltage U_0 of the cell has been included as a parameter in a Spice directive, following equation (15) to take into account the effect of the temperature.

- The reverse saturation current I_S (range of nano to micro) can also be calculated as a parameter in a Spice directive, introducing equation (10).

- Additionally, the series resistance, which is generally smaller than 0.1Ω even sometimes in mΩ, can be obtained from the module data sheet. It can be calculated as the module series resistance divided by the number of series cells.

- The rest of parameters from the data sheet have to be added as parameters.

- Otherwise, for the parallel resistor, it is large normally taken above 500-$1000\ \Omega$ and the selected value should fix the cell parameters. Therefore, some simulations with different values of R_p will be carried out to adjust it. In this project, the effect of irradiance and temperature on series and parallel resistances will not be taken into account, considering they are constant in the simulations, as the irradiance and temperature of the cells will only change in a small rank.

- The final step has been adjusting the ideality factor (any value between 1 and 2) to get the required characteristic values of the different cells (I_{SC}, V_{OC}, V_{mp}, I_{mp} and P_{mp}).

The I-V curve can be obtained by running the simulation and representing the current through the voltage source with respect to the voltage. The P-V curve can be represented adding a new plot plane with the trace $I(V_{bias}) * V_{bias}$ with respect to V_{bias}.

Therefore, by means of changing the values of $V_{irradiance}$, T, R_{series} and $R_{paralell}$ it can be easily studied their influence on the cell performance. To study the different shadowing cases, it will be changed the I_{SC} value of the current generator of the shadowed cells, taking into account that I_{SC} is proportional to the percentage of area unshaded of the cell [25].

4.1.3 String of modules of HIG laboratory modelled with LTspice IV

The string of modules at HIG laboratory has also been modelled with LTspice. These solar modules are EOPLLY 125M/72 200 W monocrystalline. Its specifications are shown in Table 2. This system has 6 modules with 72 cells and 3 bypass diodes per module. It can be seen in Figure 26.

Table 2: Specifications of HIG laboratory string modules (STC conditions)

Nominal power P_{mp} [W]	200
Maximum power voltage V_{mp} [V]	37
Maximum power current I_{mp} [A]	5.451
Open circuit voltage V_{OC} [V]	45.73
Short circuit current I_{SC} [A]	5.859
Cell efficiency [%]	15.67
Fill Factor	0.75
Power output tolerance P_{mp} [%]	±3
Series resistance of the module R_S [mΩ]	400
Nominal operation cell temperature NOCT [°C]	47 ±3
Temperature coefficient of P_{mp} [%/K]	-0.44
Temperature coefficient of V_{OC} [%/K]	-0.39
Temperature coefficient of I_{SC} [%/K]	0.06
Module dimensions (LxWxH) [mm]	1580x808x35
Cell dimensions [mm]	125x125

To do the model of this string, firstly it has been designed a cell, secondly one module with 72 cells and 3 bypass diodes properly connected and finally six modules in series have been connected.

In Figure 26, the six first modules of the string correspond to the system that has been measured using the I-V tracer. The second and the third groups of six modules correspond to a system with DC-DC optimizers and module inverters.

Figure 26: String of six modules with bypass diodes at HIG laboratory

4.1.4 Module modelled with LTspice IV

It has been simulated a mono-crystalline PV module manufactured by Windon. This module, belonging to the University of Gävle, was studied experimentally. It is shown in Figure 27.

Figure 27: PV module at the University of Gävle, manufactured by Windon

The specifications given by the manufacturer in its data sheet are showed in Table 3.

Table 3: Specifications of the university module at STC conditions

Nominal power P_{mp} [W]	265
Maximum power voltage V_{mp} [V]	31.2
Maximum power current I_{mp} [A]	8.4
Open circuit voltage V_{OC} [V]	38.6
Short circuit current I_{SC} [A]	8.9
Cell efficiency [%]	18.1
Fill Factor	0.78
Power output tolerance P_{mp} [%]	±5
Series resistance of the module R_S [mΩ]	305
Nominal operation cell temperature NOCT [°C]	47.5
Temperature coefficient of P_{mp} [%/K]	-0.382
Temperature coefficient of V_{OC} [%/K]	-0.32
Temperature coefficient of I_{SC} [%/K]	0.077
Module dimensions (LxWxH) [mm]	1665x991x43
Cell dimensions [mm]	156x156

The module model in LTspice (Figure 28) has been created using the real *single-diode* model of a solar cell described above. As it can be seen, the module has 6 columns and 10 rows, in total 60 cells, series connected. It has three bypass diodes, each of them in parallel with 2 columns of cells (20 cells).

This module allows the study of how different parameters affect the I-V curve of the module.

4.2 Experimental measurements at HIG laboratory

In order to validate the models created in LTspice, some measurements have been performed at HIG laboratory. In these paragraphs it will be explained how the instruments are used to carry out these measurements.

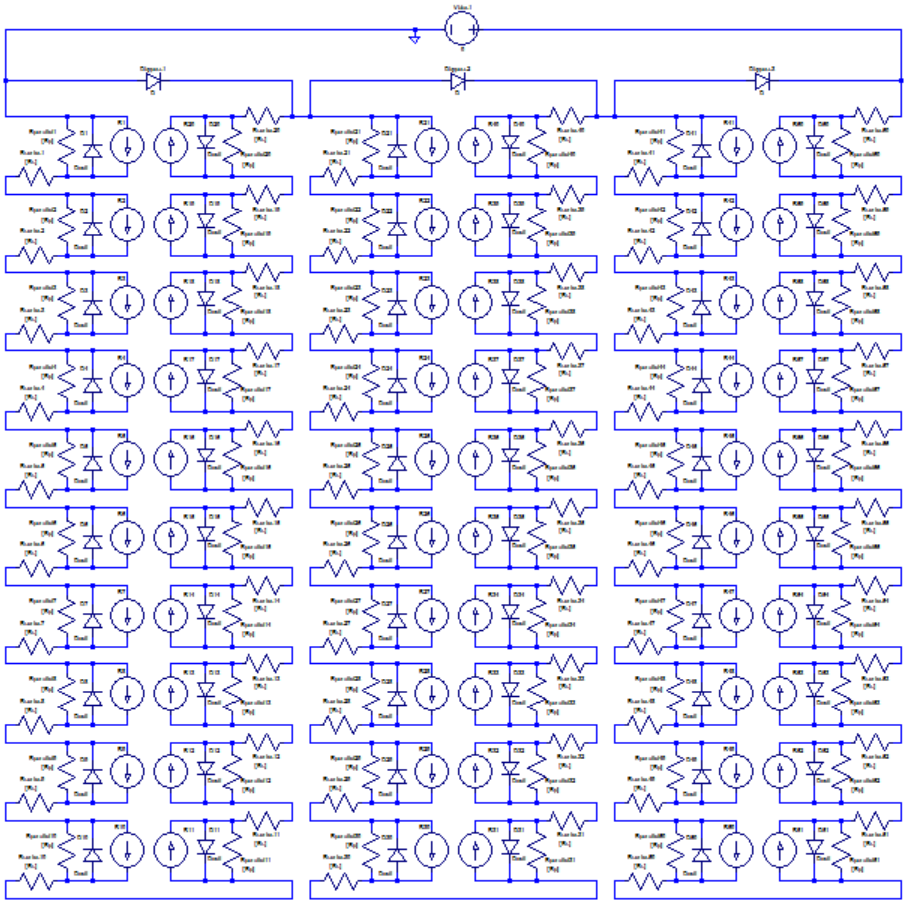

Figure 28: HIG laboratory module modelled with LTspice IV

4.2.1 I-V tracer

I-V curves or traces are measured by sweeping the load on a PV source over a range of currents and voltages. I-V tracers accomplish this by loading a PV module or string at different points across its operating range between 0 V and Voc. At each point, the output current and voltage are measured simultaneously [19]. The I-V tracer used (Figure 29) is the model EurotestPV Lite MI 3109 of METREL. To be able to download the I-V tracer measurements it is necessary having installed EuroLink PRO programme in the computer.

Figure 29: METREL I-V tracer EurotestPV Lite MI 3109

4.2.2 Pyranometer

A pyranometer is used for measuring solar irradiance on a planar surface and it is designed to measure the solar radiation flux density from the hemisphere within a wavelength range 0.3 µm to 3 µm. The pyranometer has to be located in the plane of the module that will be measured, in order to have the same tilt. The output of the pyranometer is a voltage dependent of the irradiance. In this case, the equivalence is 11.9 mV= 1000 $\frac{W}{m^2}$. The voltage has been measured with a multimeter.

4.2.3 Thermocouple sensor

To measure the temperature of the cells, it has been added a thermocouple sensor in the back of the panel. The principle is that the combination of two different metals produces a small voltage in proportion to the temperature which can then be converted into a digital signal and can be obtained in a display device.

4.3 Process and cases of study

The process that has been followed to produce this thesis and the tests accomplished at HIG laboratory are explained in this section.

The results and discussion are divided in two different parts. The first one corresponds to the string of six modules described located at HIG's laboratory roof, while the second is focused on the Windon module.

4.3.1 String of six modules at HIG laboratory

The main objective of this section is to validate the simulation models created with LTspice. In order to do that, it has been taken seven experimental measurements in the EOPLLY modules at HIG laboratory generating different kinds of shadows in the modules. In Figure 30 it can be seen how the shadows are created in the modules using an opaque tape which covers approximately the 37% of a cell, which means that each cell will generate a 63% of the current that it generates when it is unshaded.

Figure 30: Case 1.3 of study (37% of a row shaded in three modules)

Additionally, these entire seven shadow configuration will be examined to determinate how they affect to the string performance and which will be the performance of the three systems installed at HIG laboratory (bypass diodes, DC-DC optimizer and module inverter) in case its modules were sustaining these shadow configuration.

The seven cases studied starts from the base case, in which any module is shadowed. After that, an opaque tape is added in the last row of each module consecutively, taking the data for each of the cases. The different cases are enumerated below. The photos from Figure 31 to Figure 36 have been taken at the laboratory during the measurements.

- Case 1.0: not shading in the modules, base case.
- Case 1.1: 37% of a row shaded in one module.
- Case 1.2: 37% of a row shaded in two modules.
- Case 1.3: 37% of a row shaded in three modules.
- Case 1.4: 37% of a row shaded in four modules.
- Case 1.5: 37% of a row shaded in five modules.
- Case 1.6: 37% of a row shaded in six modules.

Figure 31: Experimental case 1.1

Figure 32: Experimental case 1.2

Figure 33: Experimental case 1.3

Figure 34: Experimental case 1.4

Figure 35: Experimental case 1.5

Figure 36: Experimental case 1.6

4.3.2 Effects of shading on the single laboratory module

Once the models are validated by a comparative analysis of the LTspice results with those obtained experimentally, they will be used to simulate different shadowing cases. These cases are explained below, and summarised from Figure 38 to Figure 44.

- Case 2.0: not shading, base case (Figure 37).
- Case 2.1: one cell 50% shaded.
- Case 2.2: one cell 75% shaded.
- Case 2.3: two cells 50 % shaded (cells covered by the same bypass diode).
- Case 2.4: two cells 50 % shaded (cells covered by different bypass diodes).
- Case 2.5: three cells 50 % shaded (cells covered by different bypass diodes).
- Case 2.6: one row 50% shaded.
- Case 2.7: different percentages of shadowing in each bypass circuit. Three different percentages of shadow will be study in this case:

Table 4: Percentages of shadowing studied in case 2.7

Case	First bypass circuit	Second bypass circuit	Third bypass circuit
2.7.a	70%	58%	0%
2.7.b	80%	68%	0%
2.7.c	90%	78%	0%

Figure 37: Windon module assembly during the base case experimental measurements at HIG laboratory

The module simulated in this section corresponds to the Windon module, whose specifications are given in Table 3. Two experimental measurements will be taken in the laboratory (corresponding to the first two cases) to check that the model is working correctly in the new module and to be able to adjust the ideality factor value of the module to use it in the model simulations. The assembly carried out in the laboratory can be observed in Figure 37.

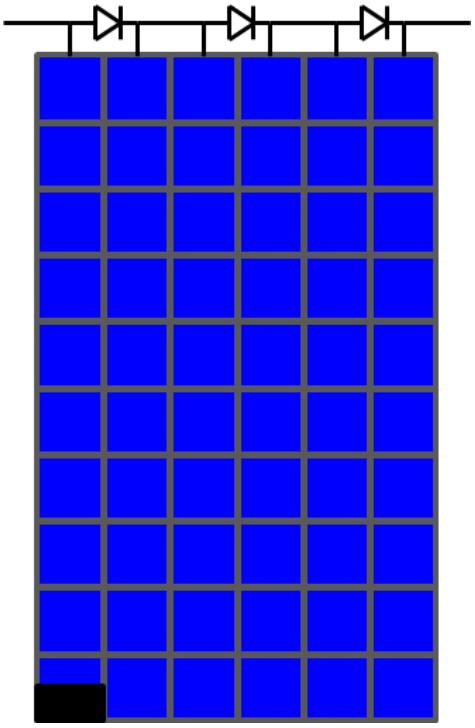

Figure 38: Shading case 2.1

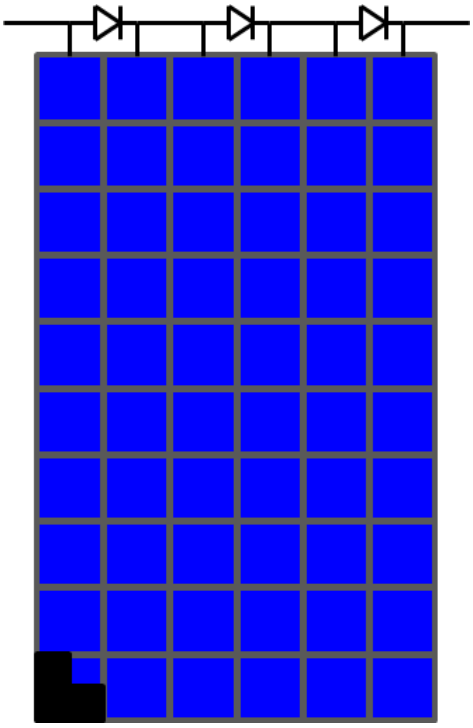

Figure 39: Shading case 2.2

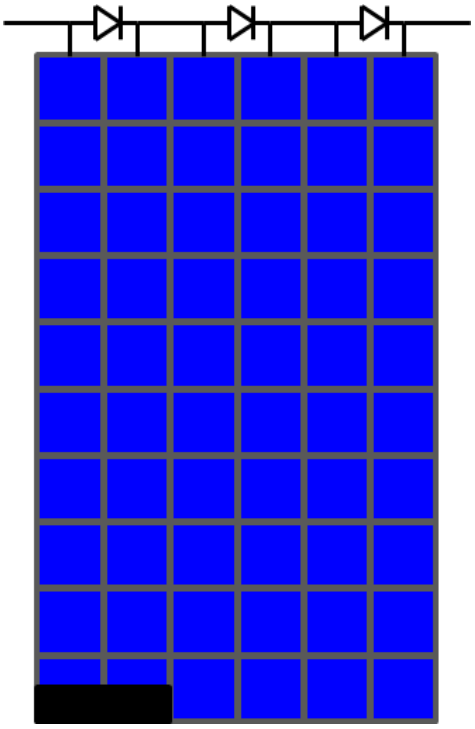

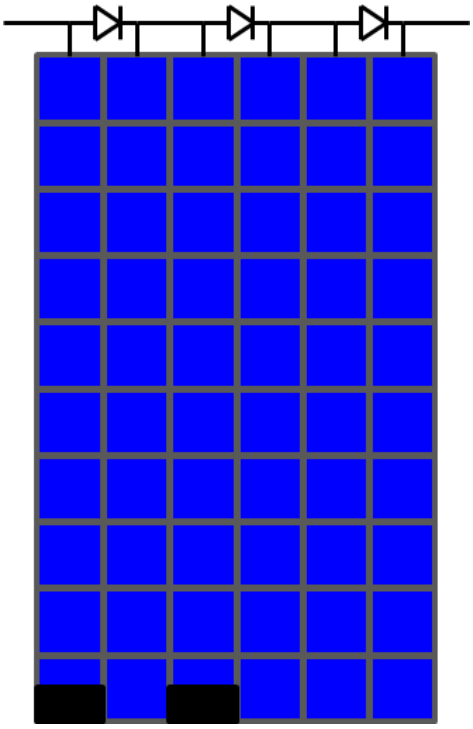

Figure 40: Shading case 2.3

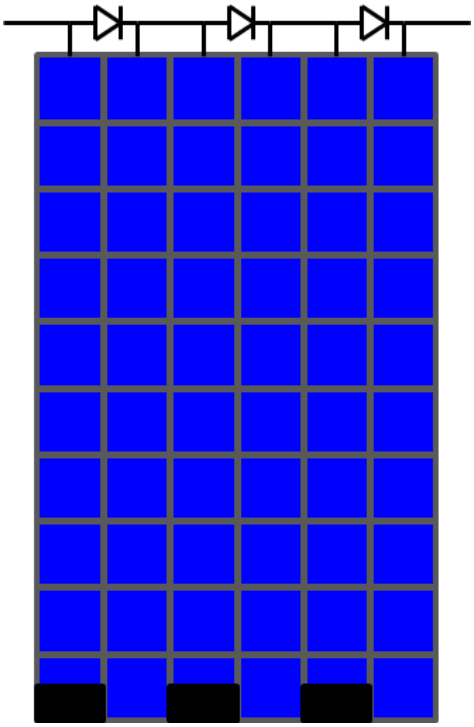

Figure 41: Shading case 2.4

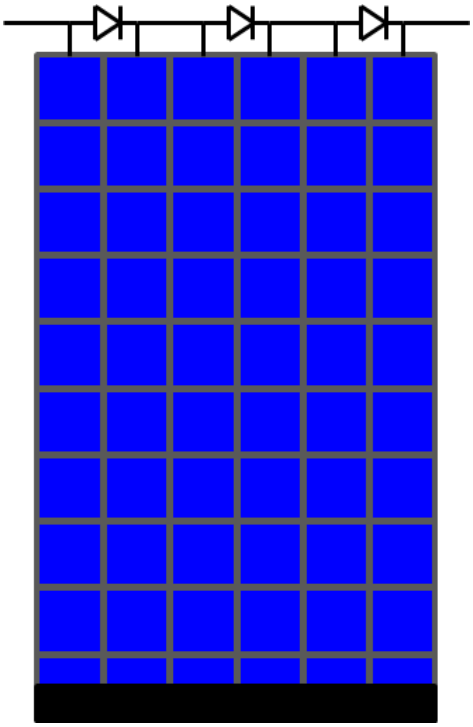

Figure 42: Shading case 2.5

Figure 43: Shading case 2.6

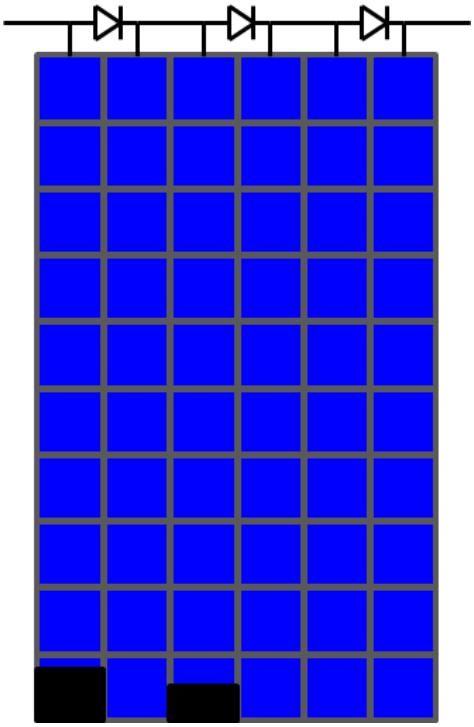

Figure 44: Shading case 2.7

Finally, it will be analysed the performance of six modules connected in series with one of its modules shadowed by means of comparing their performance in case of they have bypass diodes or DC-DC optimizers.

5. Results

This section shows the results reached following the process explained in the method.

5.1 String of six modules at HIG laboratory

Firstly, the results for the adjustment of the ideality factor n and the shunt or parallel resistance R_p are shown. After that, the simulations have been carried out and the comparison between the experimental and simulation results for all the cases can be seen from Figure 46 to Figure 52 and their summary from Table 5 to Table 13.

5.1.1 Adjustment of R_p and n

First of all, the I-V curve obtained experimentally has been used to calculate the ideality factor, n and the parallel resistance, R_p.

As it can be seen in Figure 45, the influence of R_p is negligible. The three curves with ideality factor equal to 1.28 and R_p equal to 1000, 500 and 250 Ω respectively are superimposed. For the following simulations R_p will be selected equal to 1000 Ω.

On the other hand, it can be seen that the influence of the ideality factor is appreciable. The value that better agrees with the experimental curve is n=1.8, so this is the value that will be used in the LTspice model created.

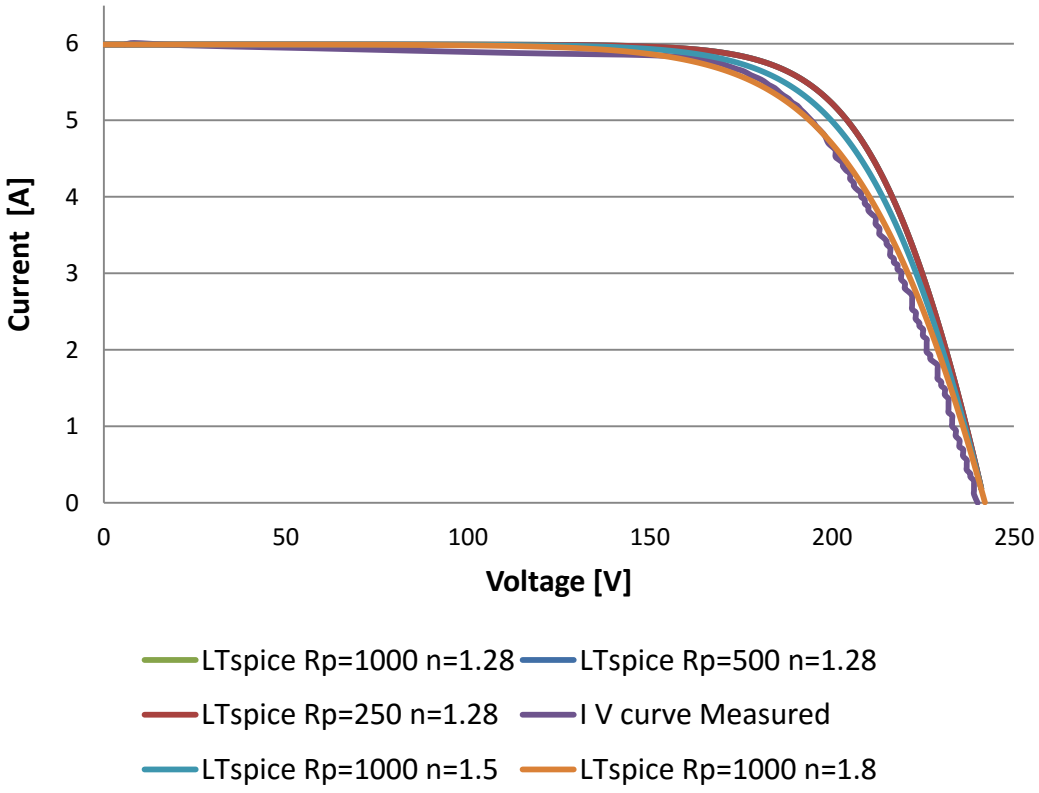

Figure 45: I-V curves for different n and Rp values in comparison with the measured I-V curve

5.1.2 Case 1.0: not shading in the modules, base case

The comparison between the experimental and simulation results carried out for case 1.0 is shown in Figure 46 and in Table 5.

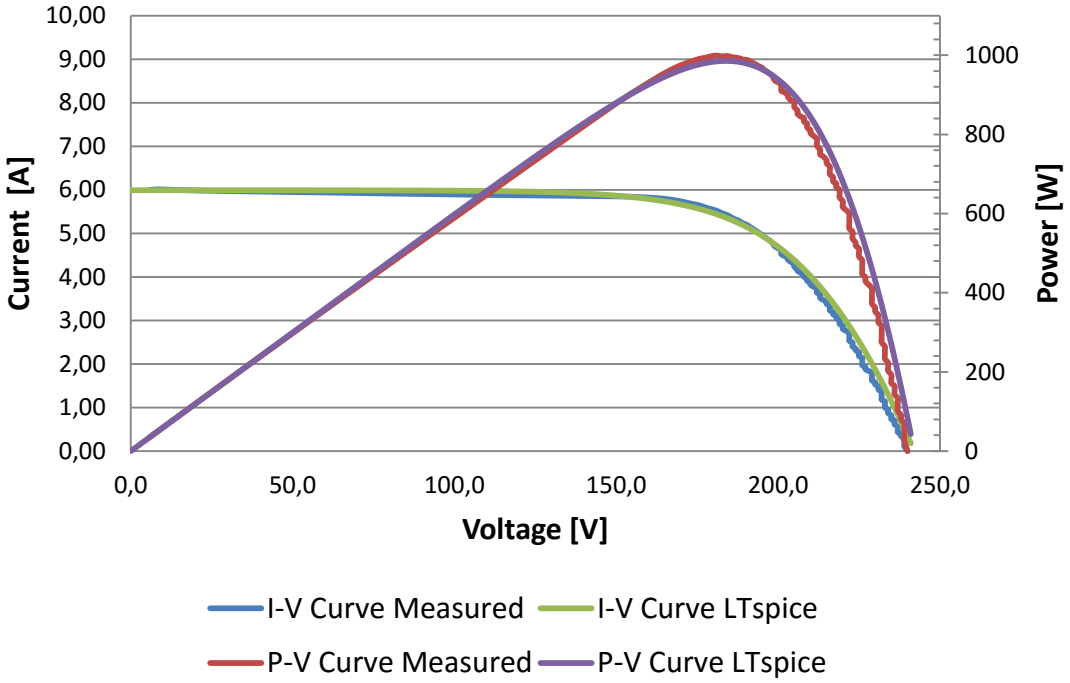

Figure 46: Comparison of simulation and experimental curves for case 1.0

Table 5: Comparison of simulated and experimental results for case 1.0

	LTspice Simulation	**HIG Laboratory Experimental**	$\lvert\Delta_{abs}\rvert$	$\lvert\Delta_{rel}\rvert$ (%)
G $\left[\frac{W}{m^2}\right]$	1003,00		0,00	
T [°C]	57,13		0,00	
V_{oc} **[V]**	242,00	240,00	2,00	0,83
I_{sc} **[A]**	5,99	5,99	0,00	0,00
V_{mp} **[V]**	184,00	181,30	2,70	1,49
I_{mp} **[A]**	5,36	5,51	0,15	2,72
P_{max} **[W]**	985,47	998,96	13,49	1,35
FF (%)	68,04	69,49	1,45	2,09
η_{cell} **(%)**	14,57	14,76	0,19	1,27

5.1.3 Case 1.1: 37% of a row shaded in one module

The comparison between the experimental and simulation results carried out for case 1.1 is shown in Figure 47 and in Table 6.

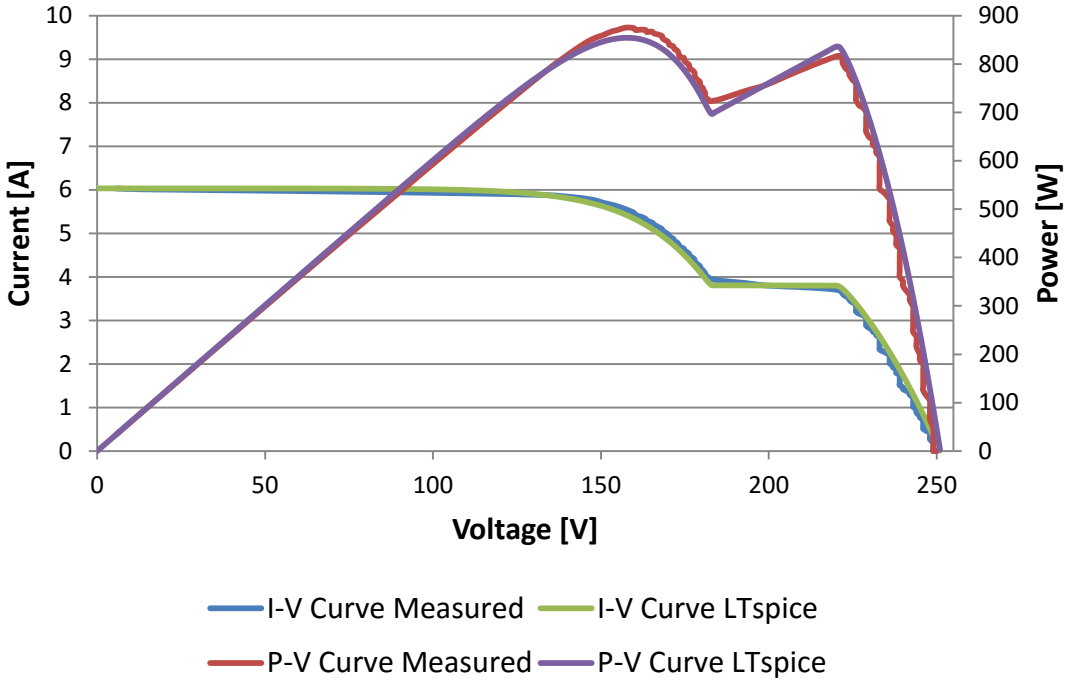

Figure 47: Comparison of simulation and experimental curves for case 1.1

Table 6: Comparison of simulated and experimental results for case 1.1

	LTspice Simulation	**HIG Laboratory Experimental**	$\lvert\Delta_{abs}\rvert$	$\lvert\Delta_{rel}\rvert$ (%)
G $\left[\frac{W}{m^2}\right]$	1015,00		0,00	
T [°C]	48,75		0,00	
V_{oc} **[V]**	251,07	249,00	2,07	0,83
I_{sc} **[A]**	6,03	6,03	0,00	0,00
V_{mp} **[V]**	158,00	158,80	0,80	0,50
I_{mp} **[A]**	5,41	5,51	0,10	1,81
P_{max} **[W]**	854,11	874,98	20,87	2,39
FF (%)	56,46	58,28	1,82	3,11
η_{cell} **(%)**	12,48	12,77	0,29	2,31

5.1.4 Case 1.2: 37% of a row shaded in two modules

The comparison between the experimental and simulation results carried out for case 1.2 is shown in Figure 48 and in Table 7.

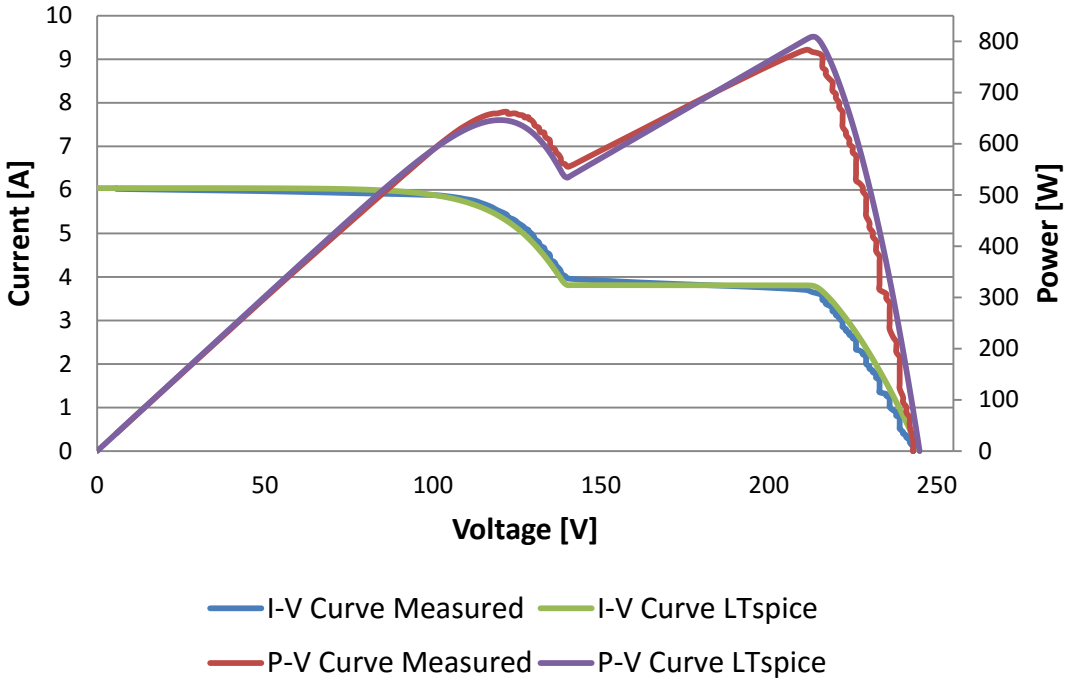

Figure 48: Comparison of simulation and experimental curves for case 1.2

Table 7: Comparison of simulated and experimental results for case 1.2

	LTspice Simulation	**HIG Laboratory Experimental**	$\lvert\Delta_{abs}\rvert$	$\lvert\Delta_{rel}\rvert$ (%)
G $\left[\frac{W}{m^2}\right]$	1013,00		0,00	
T [°C]	54,35		0,00	
V_{oc} **[V]**	244,93	243,00	1,93	0,79
I_{sc} **[A]**	6,04	6,04	0,00	0,01
V_{mp} **[V]**	213,00	211,00	2,00	0,95
I_{mp} **[A]**	3,80	3,70	0,10	2,62
P_{max} **[W]**	808,73	783,00	25,73	3,29
FF (%)	54,67	53,19	1,48	2,78
η_{cell} **(%)**	11,83	11,42	0,41	3,59

5.1.5 Case 1.3: 37% of a row shaded in three modules

The comparison between the experimental and simulation results carried out for case 1.3 is shown in Figure 49 and in Table 8.

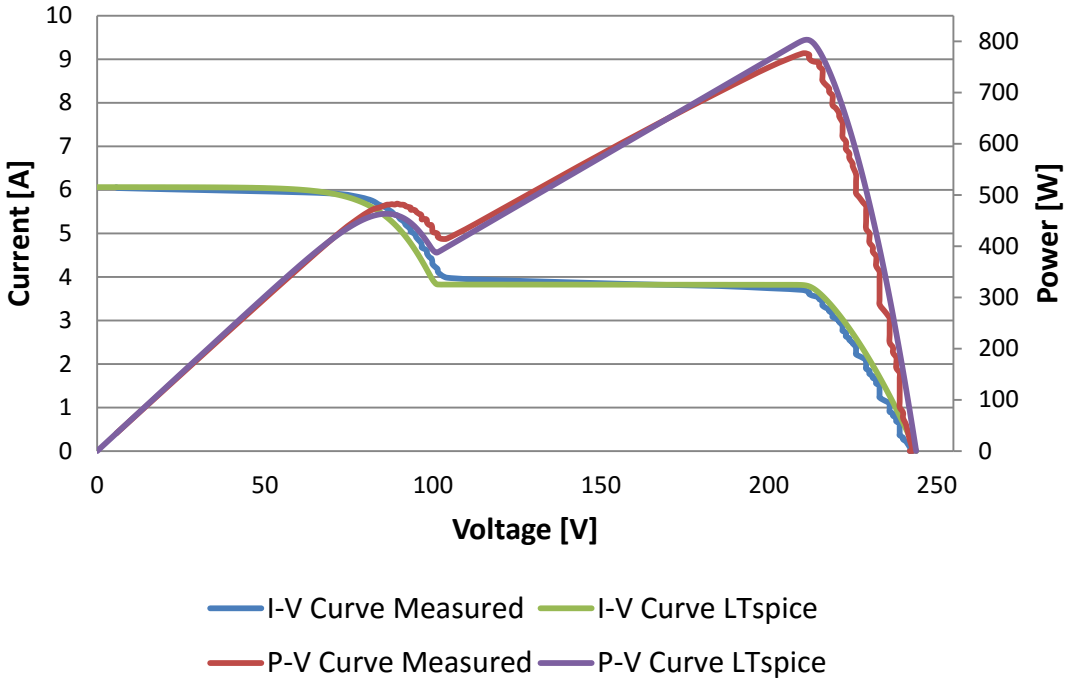

Figure 49: Comparison of simulation and experimental curves for case 1.3

Table 8: Comparison of simulated and experimental results for case 1.3

	LTspice Simulation	**HIG Laboratory Experimental**	$\lvert\Delta_{abs}\rvert$	$\lvert\Delta_{rel}\rvert$ (%)
G $\left[\frac{W}{m^2}\right]$	1016,00		0,00	
T [°C]	55,25		0,00	
V_{oc} **[V]**	243,91	242,00	1,91	0,79
I_{sc} **[A]**	6,06	6,06	0,00	0,00
V_{mp} **[V]**	211,00	210,00	1,00	0,48
I_{mp} **[A]**	3,80	3,70	0,10	2,81
P_{max} **[W]**	802,75	776,00	26,75	3,45
FF (%)	54,30	52,98	1,32	2,49
η_{cell} **(%)**	11,70	11,33	0,37	3,30

5.1.6 Case 1.4: 37% of a row shaded in four modules

The comparison between the experimental and simulation results carried out for case 1.4 is shown in Figure 50 and in Table 9.

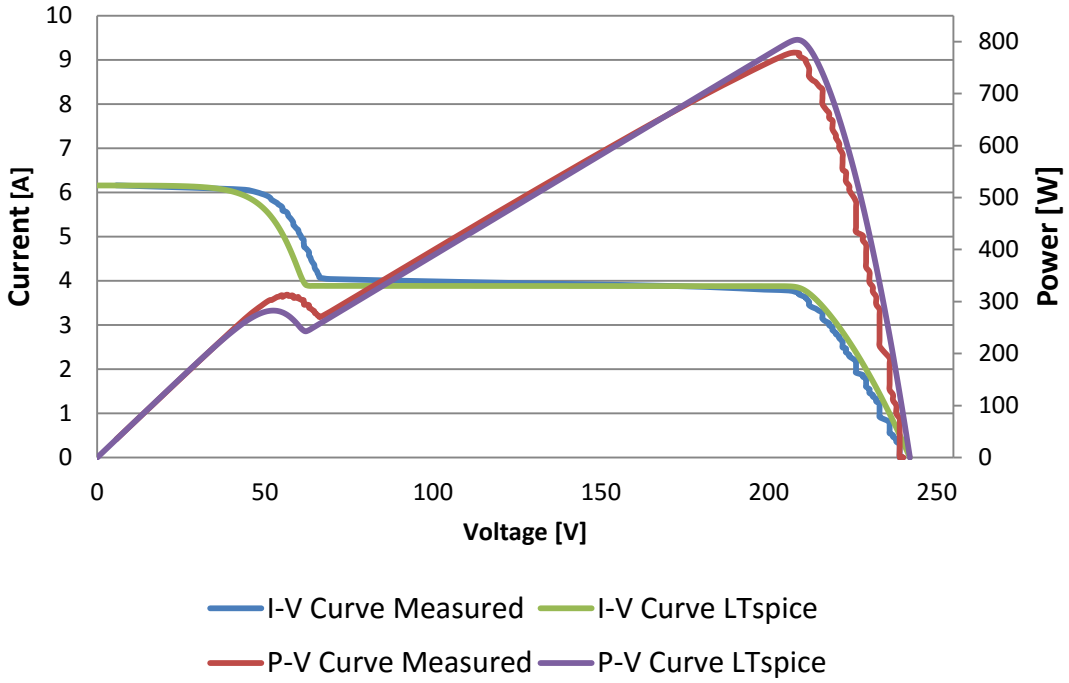

Figure 50: Comparison of simulation and experimental curves for case 1.4

Table 9: Comparison of simulated and experimental results for case 1.4

	LTspice Simulation	**HIG Laboratory Experimental**	$\lvert\Delta_{abs}\rvert$	$\lvert\Delta_{rel}\rvert$ (%)
G $\left[\frac{W}{m^2}\right]$	1031,00		0,00	
T [°C]	57,15		0,00	
V_{oc} **[V]**	242,05	240,00	2,05	0,85
I_{sc} **[A]**	6,16	6,16	0,00	0,00
V_{mp} **[V]**	209,00	209,00	0,00	0,00
I_{mp} **[A]**	3,84	3,72	0,12	3,23
P_{max} **[W]**	803,17	778,00	25,17	3,24
FF (%)	53,83	52,59	1,24	2,35
η_{cell} **(%)**	11,53	11,17	0,36	3,23

5.1.7 Case 1.5: 37% of a row shaded in five modules

The comparison between the experimental and simulation results carried out for case 1.5 is shown in Figure 51 and in Table 10.

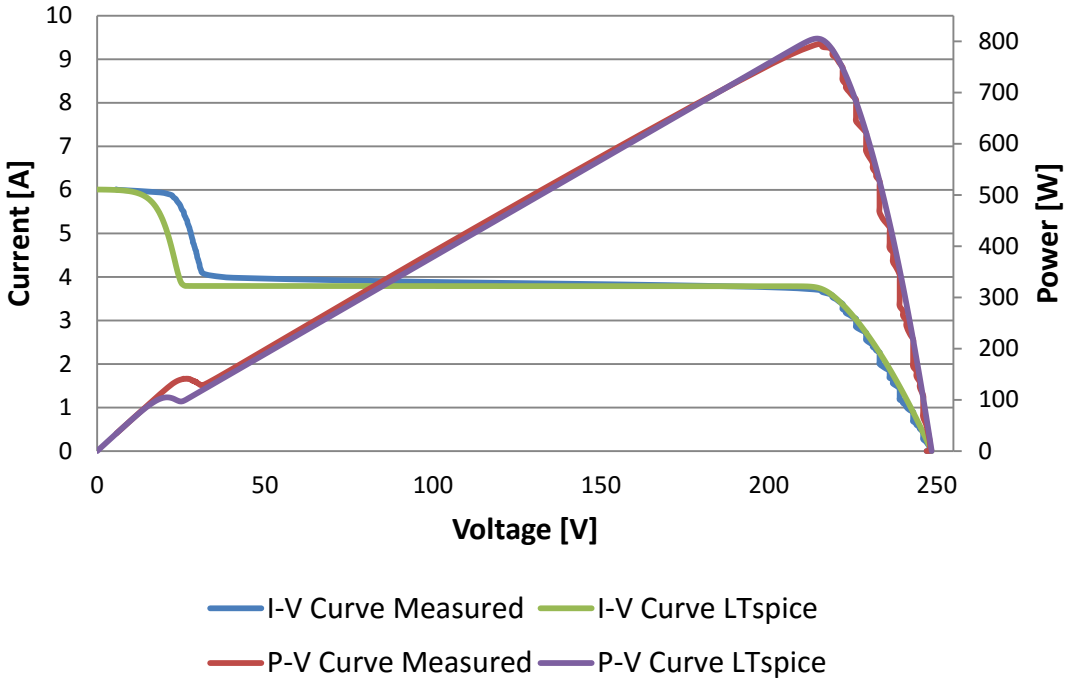

Figure 51: Comparison of simulation and experimental curves for case 1.5

Table 10: Comparison of simulated and experimental results for case 1.5

	LTspice Simulation	HIG Laboratory Experimental	$\lvert\Delta_{abs}\rvert$	$\lvert\Delta_{rel}\rvert$ (%)
G $\left[\frac{W}{m^2}\right]$	1010,00		0,00	
T [°C]	50,55		0,00	
V_{oc} [V]	248,53	247,00	1,53	0,62
I_{sc} [A]	6,01	6,01	0,00	0,00
V_{mp} [V]	214,00	215,00	1,00	0,47
I_{mp} [A]	3,76	3,70	0,06	1,62
P_{max} [W]	804,95	795,00	9,95	1,25
FF (%)	53,87	53,59	0,28	0,53
η_{cell} (%)	11,80	11,67	0,13	1,15

5.1.8 Case 1.6: 37% of a row shaded in six modules

The comparison between the experimental and simulation results carried out for case 1.6 is shown in Figure 52 and in Table 11.

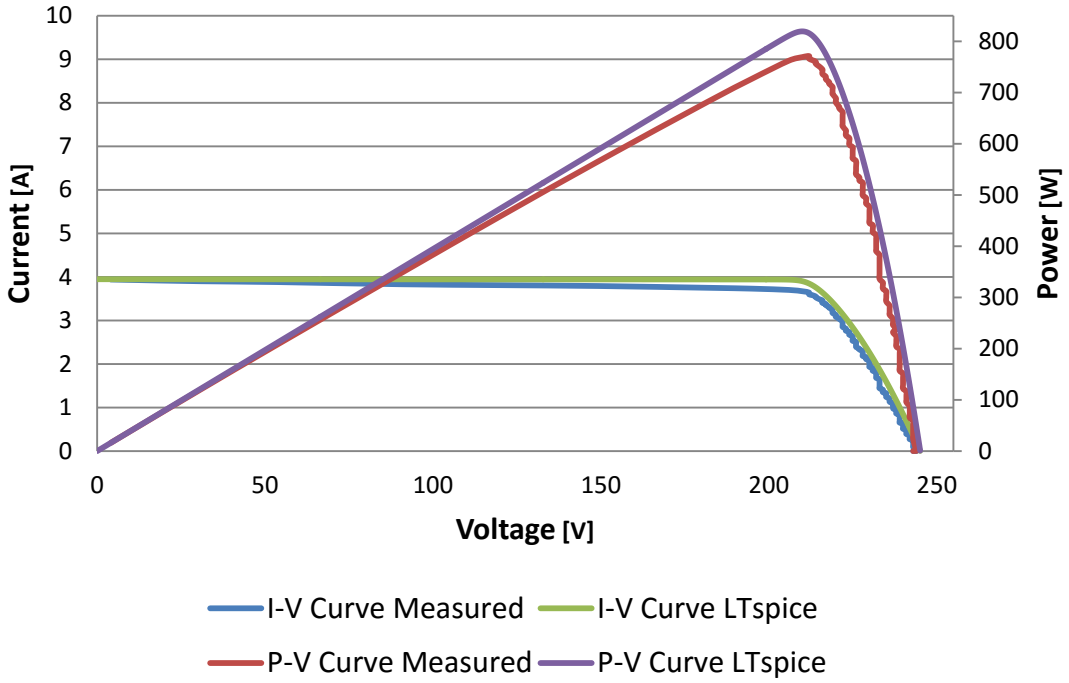

Figure 52: Comparison of simulation and experimental curves for case 1.6

Table 11: Comparison of simulated and experimental results for case 1.6

	LTspice Simulation	**HIG Laboratory Experimental**	$\lvert\Delta_{abs}\rvert$	$\lvert\Delta_{rel}\rvert$ (%)
G $\left[\frac{W}{m^2}\right]$	1049,00		0,00	
T [°C]	54,35		0,00	
V_{oc} **[V]**	245,10	243,00	2,10	0,86
I_{sc} **[A]**	3,95	3,94	0,01	0,25
V_{mp} **[V]**	209,90	212,00	2,10	0,99
I_{mp} **[A]**	3,90	3,64	0,26	7,14
P_{max} **[W]**	819,19	771,00	48,19	6,25
FF (%)	84,55	80,60	3,95	4,91
η_{cell} **(%)**	11,56	10,90	0,66	6,08

5.1.9 Simulation results at STC conditions

Registration of an IV-curve during Standard Testing Conditions means that the solar irradiance G=1000W/m² at normal incidence and the module temperature T=25°C. The MPP in STC condition for all the cases is summarised in Table 12.

Table 12: Simulation results of the MPP for all the cases at STC conditions

Case number	V_{mp} [V]	I_{mp} [A]	P_{max} [W]
1.0	214,99	5,33	1145,90
1.1	176,96	5,32	941,43
1.2	243,99	3,68	897,88
1.3	243,00	3,68	894,24
1.4	242,00	3,67	888,14
1.5	241,01	3,67	884,51
1.6	240,50	3,66	880,23

5.1.10 MPP of the DC-DC Optimizer and the module inverter

The theoretical power obtained when a DC-DC optimizer or a module inverter is installed is calculated from the data in Table 12, taking into account that they get the maximum power of each of the modules. The results are summarized in Table 13.

Table 13: MPP of the DC-DC Optimizer and at STC conditions and comparison with bypass diodes system

Case number	P_{max} [W] String of modules with diodes	P_{max} [W] String of modules with diodes and optimizer	Power difference between optimizer and diodes system (%)
1.0	1145,90	1145,90	0,0
1.1	941,43	1101,62	17,0
1.2	897,88	1057,34	17,8
1.3	894,24	1013,06	13,3
1.4	888,14	968,79	9,1
1.5	884,51	924,51	4,5
1.6	880,23	880,23	0,0

5.2 Effects of shading on the single laboratory module

Firstly, it will be adjust the ideality factor and the parallel resistor and in the following sections it will be analysed eight different configurations of shading from Figure 54 to Figure 64 and from Table 15 to Table 18.

5.2.1 Adjustment of R_p and n

Firstly, it has to be calculated R_p and n values by means of comparing the simulation and the experimental results, like it has been done in the first section. Figure 53 shows the I-V curves for different values of n and R_p and Table 14 summarises the main points of these curves.

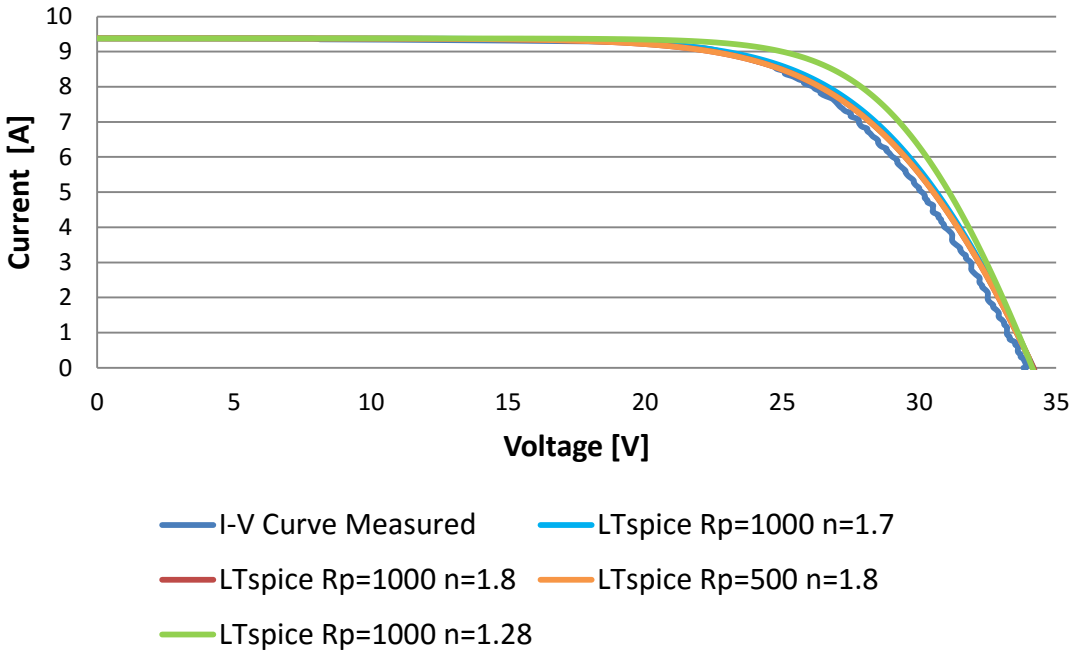

Figure 53: I-V curves for different n and Rp values in comparison with the measured I-V curve

Table 14: MPP for different n and Rp values for simulations and measurements

		I_{mp} [A]	V_{mp} [V]	P_{max} [W]
Measured		9,12	24,20	220,704
R=1000 Ω	**n=1.28**	8,65	26,40	228,36
	n=1.7	8,88	25,60	227,328
	n=1.8	8,92	25,40	226,568
R=500 Ω	**n=1.8**	8,67	26,00	225,42

5.2.2 Module validation: case 2.0 (not shading in the module)

The comparison between the experimental and simulation results carried out for case 2.0 is shown in Figure 54 and in Table 15.

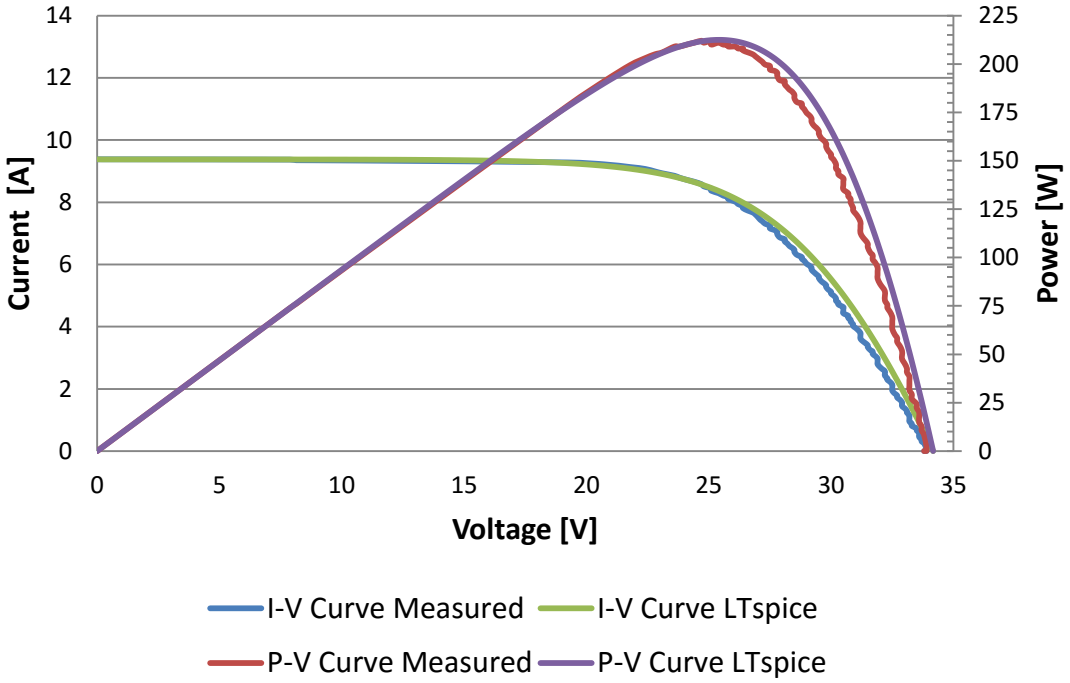

Figure 54: Comparison of simulation and experimental curves for case 2.0

Table 15: Comparison of simulated and experimental results for case 2.0

	LTspice Simulation	HIG Laboratory Experimental	$\lvert\Delta_{abs}\rvert$	$\lvert\Delta_{rel}\rvert$ (%)
G $\left[\frac{W}{m^2}\right]$	1023,00		0,00	
T [°C]	63,85		0,00	
V_{oc} [V]	34,17	33,80	0,37	1,09
I_{sc} [A]	9,38	9,38	0,00	0,00
V_{mp} [V]	25,40	24,70	0,70	2,83
I_{mp} [A]	8,36	8,58	0,22	2,56
P_{max} [W]	212,46	211,93	0,53	0,25
FF (%)	66,25	66,84	0,59	0,89
η_{cell} (%)	14,22	14,19	0,03	0,20

5.2.3 Module validation: case 2.1 (50%of a cell shaded)

The comparison between the experimental and simulation results carried out for case 2.1 is shown in Figure 55 and in Table 16.

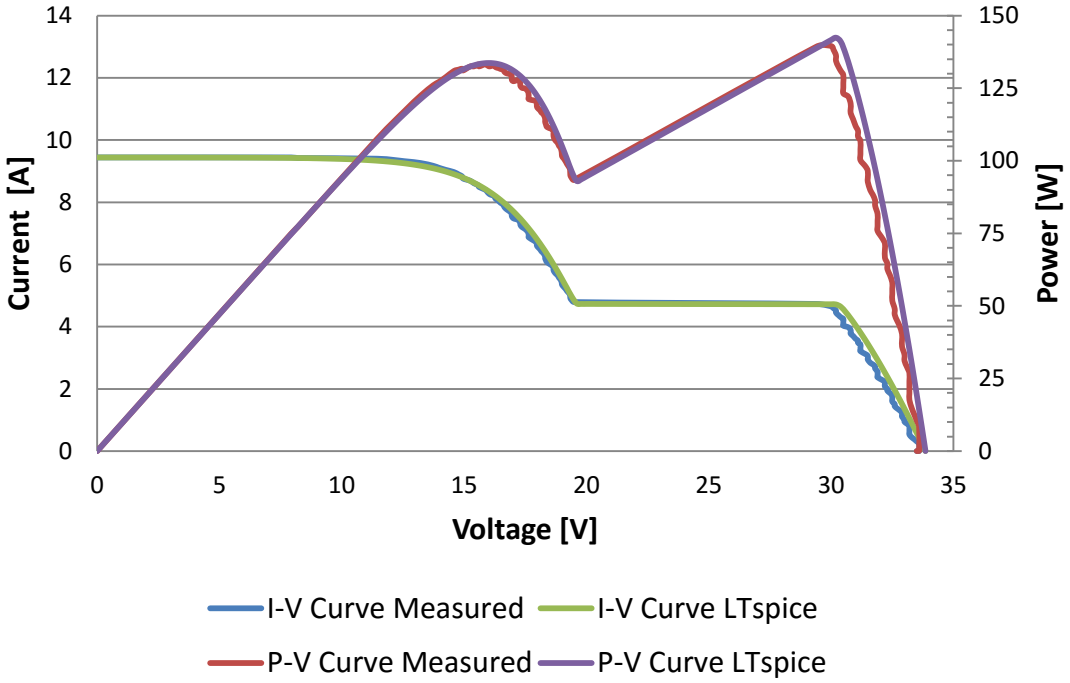

Figure 55: Comparison of simulation and experimental curves for case 2.1

Table 16: Comparison of simulated and experimental results for case 2.1

	LTspice Simulation	HIG Laboratory Experimental	$\lvert\Delta_{abs}\rvert$	$\lvert\Delta_{rel}\rvert$ (%)
G $\left[\frac{W}{m^2}\right]$	1028,00		0,00	
T [°C]	66,25		0,00	
V_{oc} [V]	33,86	33,60	0,26	0,77
I_{sc} [A]	9,44	9,44	0,00	0,00
V_{mp} [V]	30,20	30,00	0,20	0,67
I_{mp} [A]	4,71	4,65	0,06	1,29
P_{max} [W]	142,38	139,50	2,88	2,06
FF (%)	44,50	43,98	0,52	1,18
η_{cell} (%)	9,48	9,29	0,18	1,97

5.2.4 Case 2.0: not shading in the module, base case

The LTspice simulated I-V and P-V curves for case 2.0 are represented in Figure 56.

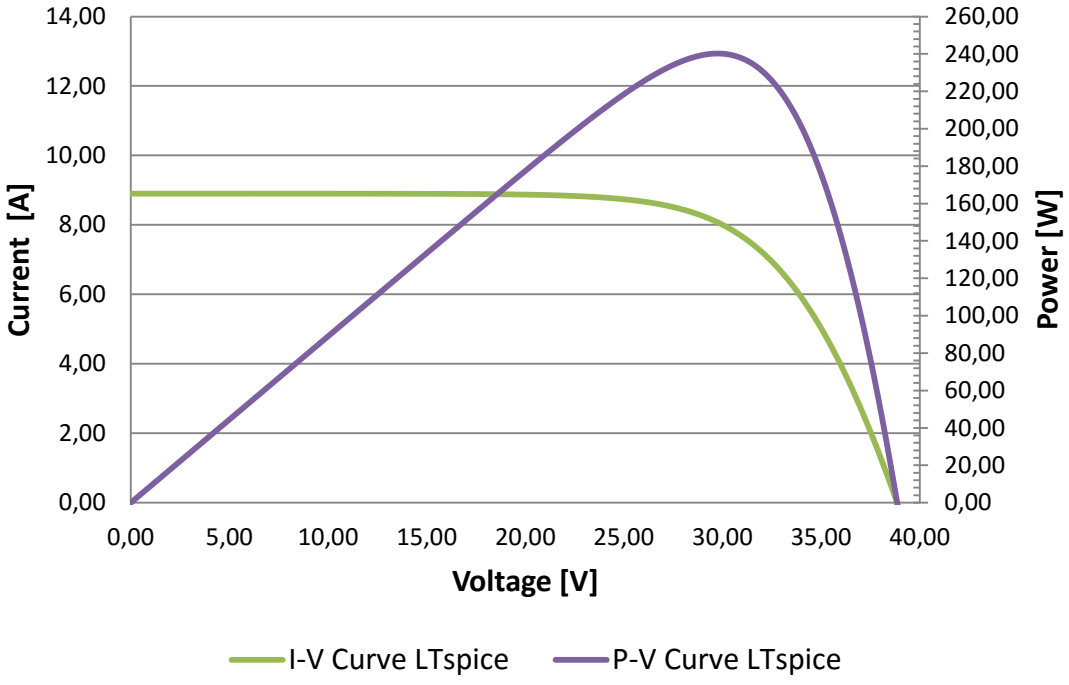

Figure 56: LTspice simulations for case 2.0 at STC conditions

5.2.5 Case 2.1: 50% of a cell shaded

The LTspice simulated I-V and P-V curves for case 2.1 are represented in Figure 57.

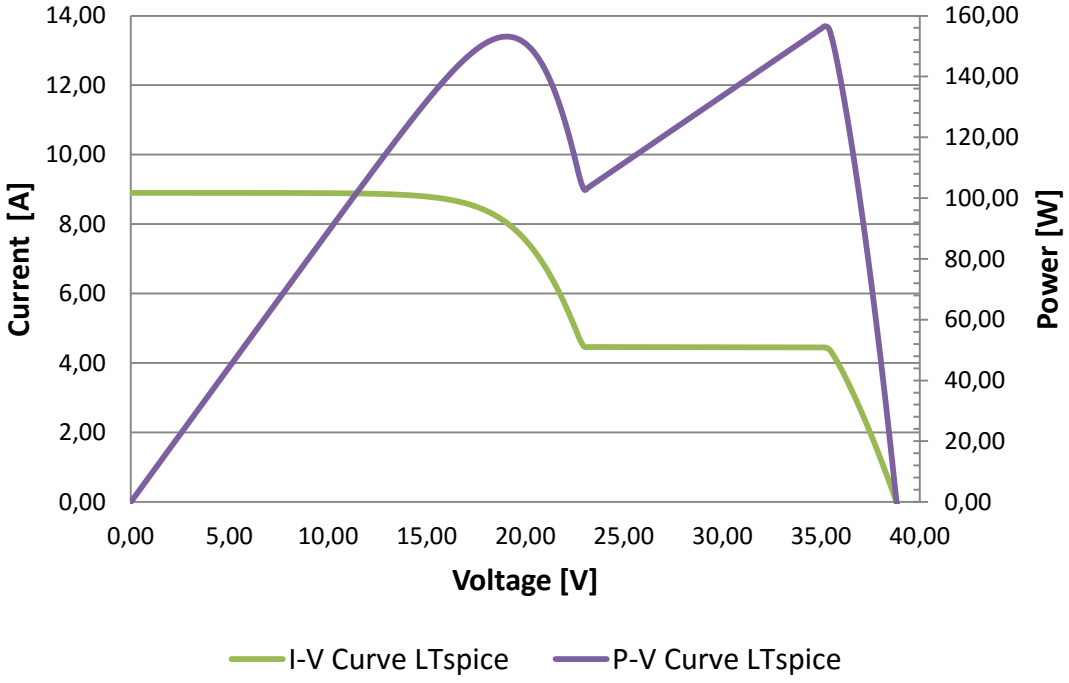

Figure 57: LTspice simulations for case 2.1 at STC conditions

5.2.6 Case 2.2: 75% of a cell shaded

The LTspice simulated I-V and P-V curves for case 2.2 are represented in Figure 58.

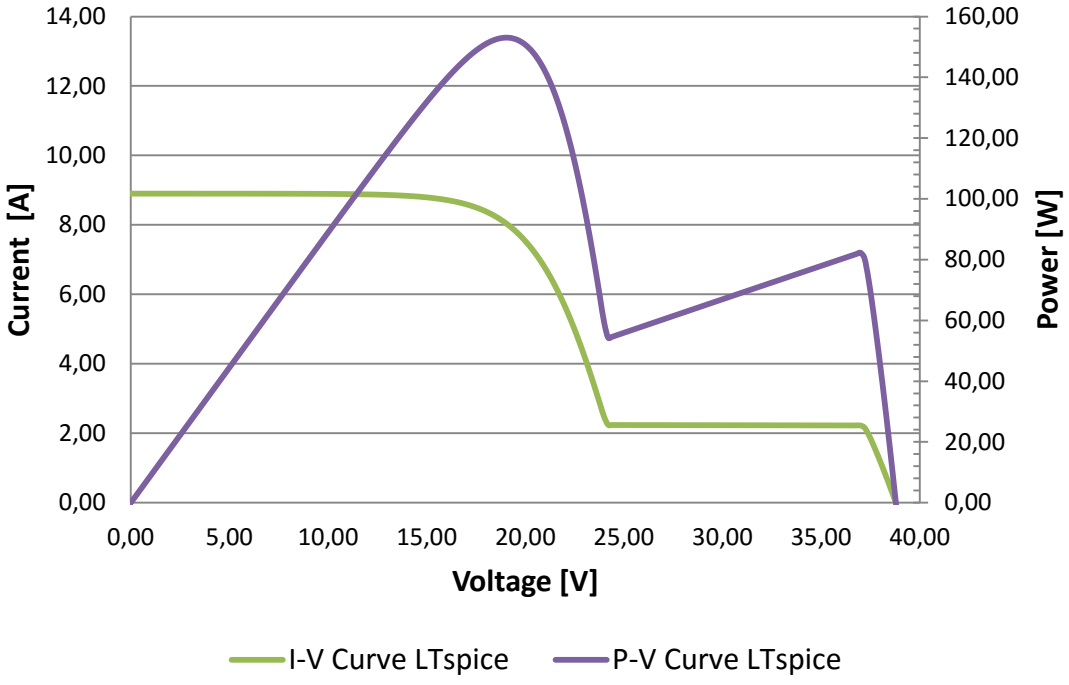

Figure 58: LTspice simulations for case 2.2 at STC conditions

5.2.7 Case 2.3: 50 % of two cells shaded (same bypass circuit)

The LTspice simulated I-V and P-V curves for case 2.3 are represented in Figure 59.

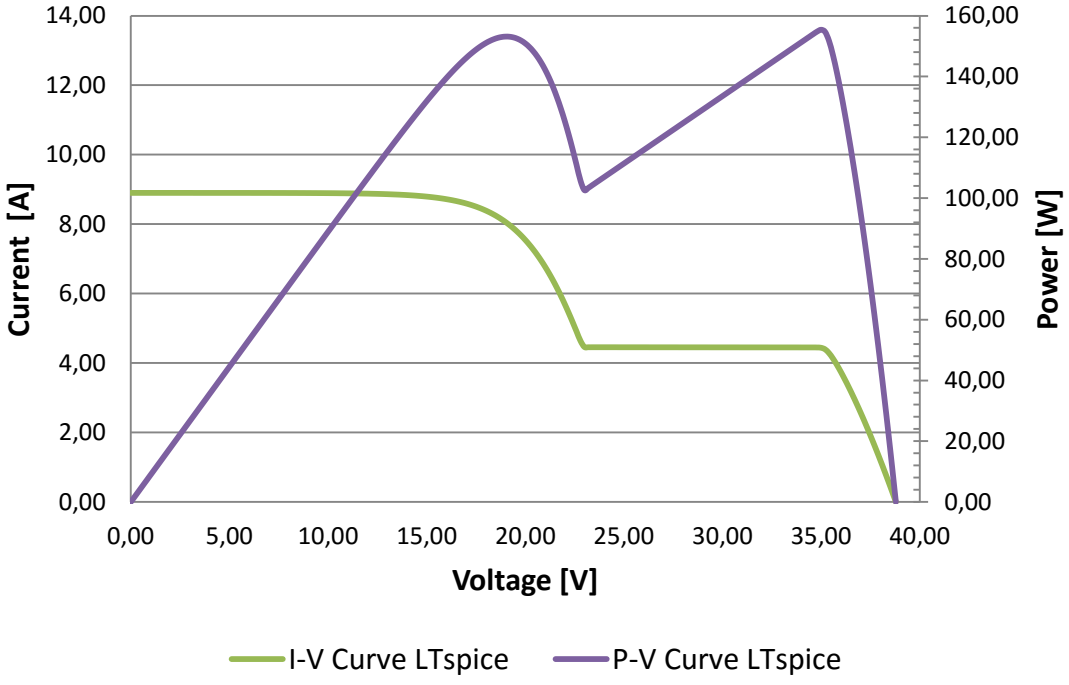

Figure 59: LTspice simulations for case 2.3 at STC conditions

5.2.8 Case 2.4: 50 % of two cells shaded (different bypass circuit)

The LTspice simulated I-V and P-V curves for case 2.4 are represented in Figure 60.

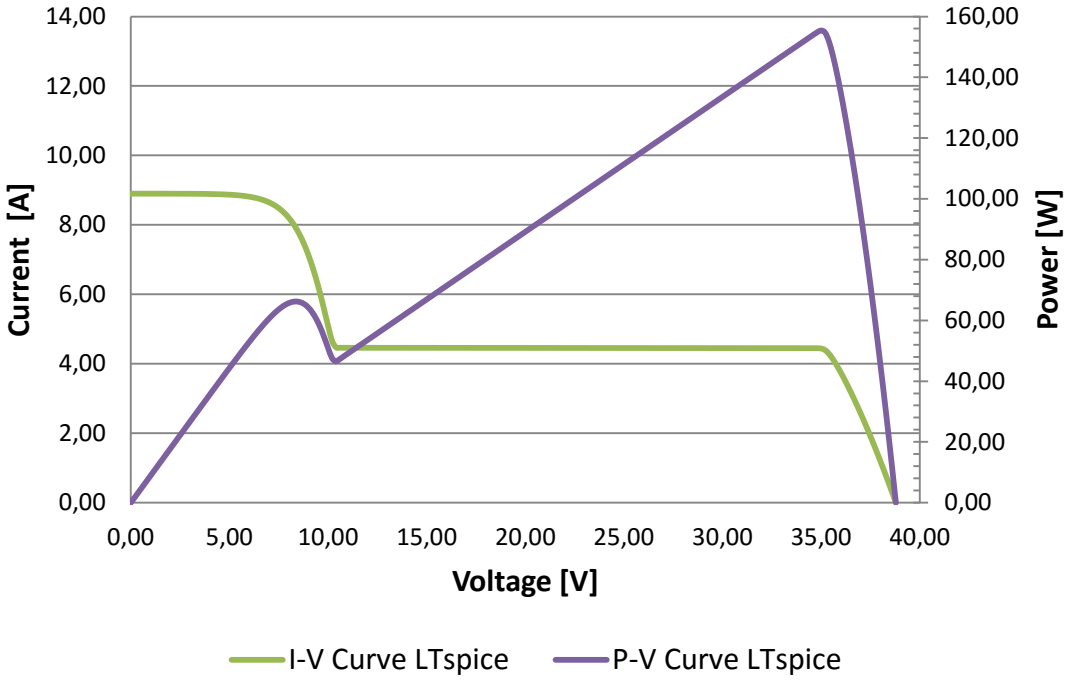

Figure 60: LTspice simulations for case 2.4 at STC conditions

5.2.9 Case 2.5: 50 % of three cells shaded (different bypass circuit)

The LTspice simulated I-V and P-V curves for case 2.5 are represented in Figure 61.

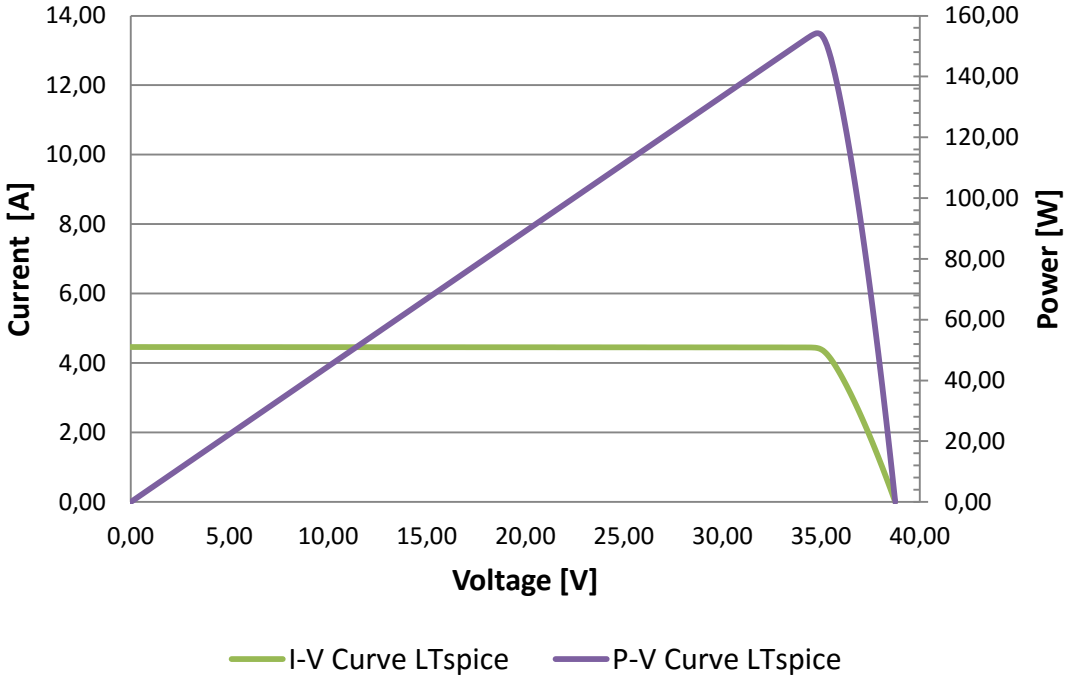

Figure 61: LTspice simulations for case 2.5 at STC conditions

5.2.10 Case 2.6: 50% of one row shaded

The LTspice simulated I-V and P-V curves for case 2.6 are represented in Figure 62.

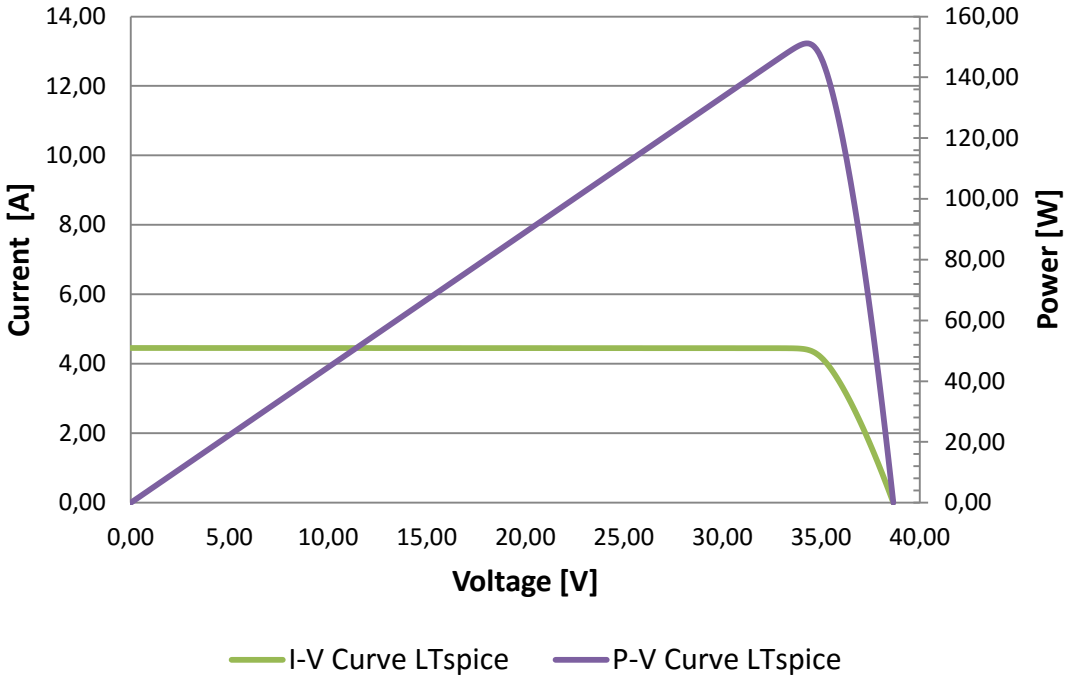

Figure 62: LTspice simulations for case 2.6 at STC conditions

5.2.11 Case 2.7: different percentages of shadowing in each bypass circuit

The LTspice simulated I-V and P-V curves for case 2.7 are represented in Figure 63.

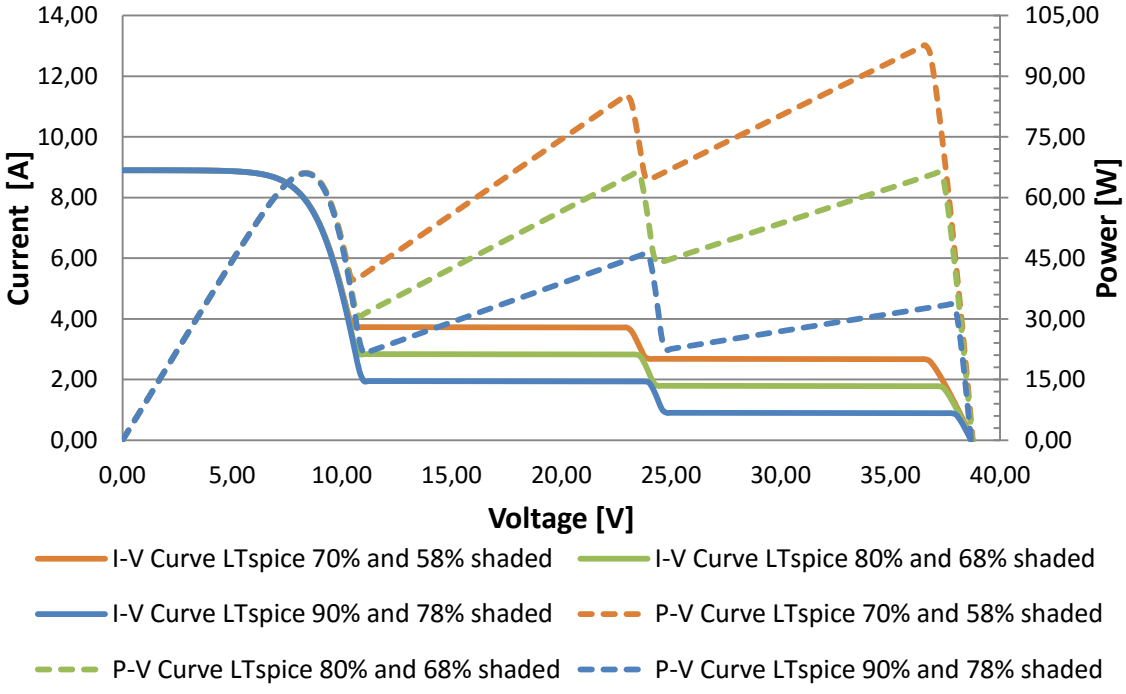

Figure 63: LTspice simulations for cases 2.7.a, b and c at STC conditions

5.2.12 Simulation results at STC conditions

Table 17 summarised the MPP in each of the cases obtained by LTspice simulations from cases 2.0 to 2.7 at STC conditions. All the simulations have been done at STC conditions to facilitate their comparison.

Table 17: Simulation results of the MPP for all the module cases at STC conditions

Case number		V_{mp} [V]	I_{mp} [A]	P_{max} [W]
2.0		29,80	8,06	240,20
2.1		35,20	4,45	156,57
2.2		19,00	8,06	153,05
2.3		35,00	4,44	155,40
2.4		35,00	4,44	155,40
2.5		34,80	4,43	154,25
2.6		34,20	4,42	151,12
2.7	**a**	36,60	2,67	97,62
	b	8,40	7,86	66,00
	c	8,40	7,86	66,00

5.2.13 Comparison chart with all the cases curves

Finally, all the charts presented above have been combined in Figure 64. Although having so many curves in the same graphic can makes it difficult to evaluate it, this chart gives a better point of view of the magnitude of each curve and it helps to compare the different cases.

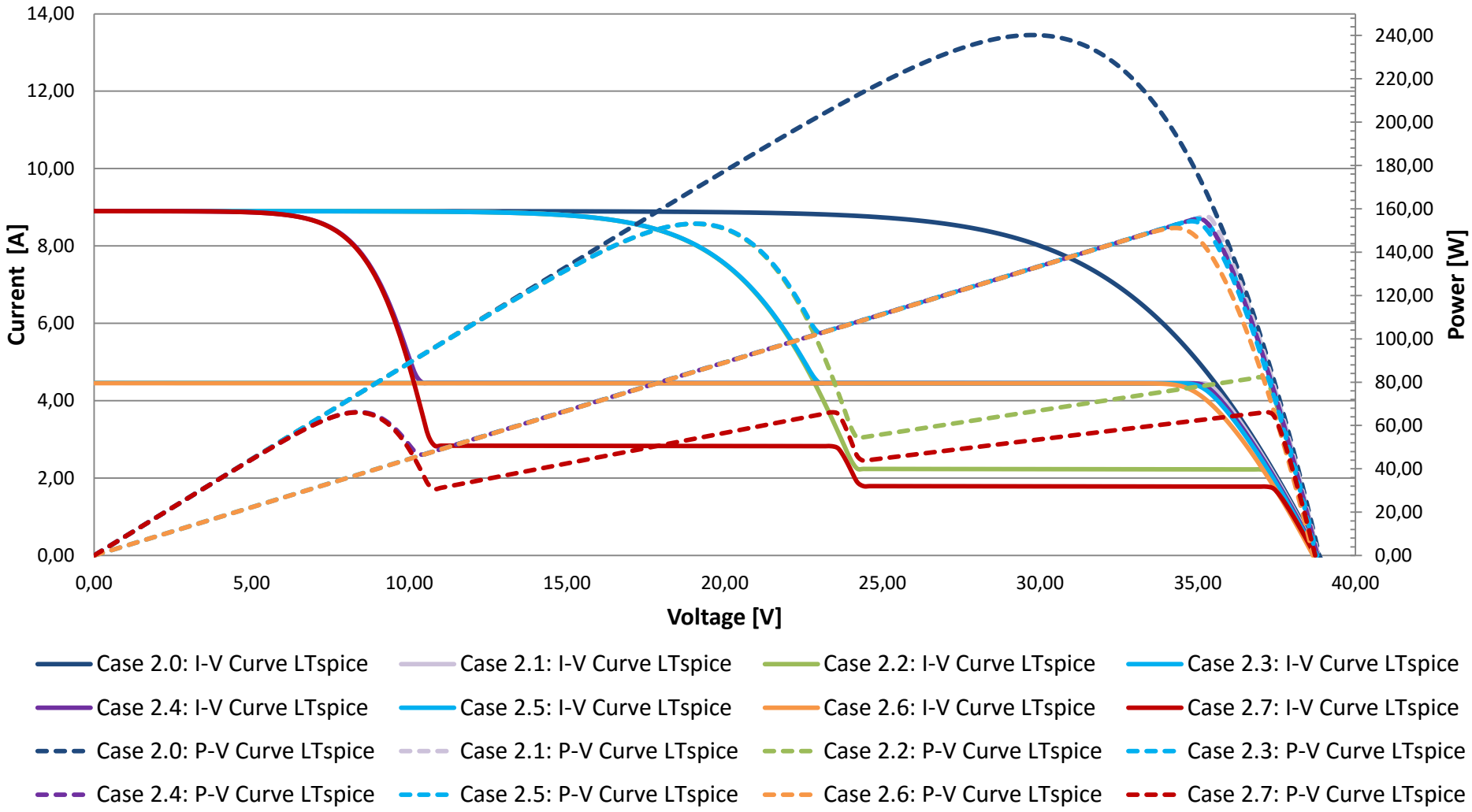

Figure 64: LTspice simulations for the eight shading cases studied in the module at STC conditions

5.2.14 Performance of systems affected by shadows

Table 18 synthesises the maximum power output that would be obtained from a string of six modules Windon connected in series when one of the modules is shaded. The shadowing configurations studied are the same than in the sections before, from 2.0 to 2.7. Two different systems are compared: on the one hand a system that only have bypass diodes in the modules and on the other hand a system which has an additional optimizer in each of the modules.

Table 18: Performance of the string of six modules with and without optimizer at STC conditions

Case number		P_{max} [W]		
		String of modules with diodes	String of modules with diodes and module optimizer	Difference between optimizer and diodes system (%)
2.0		1441,2	1441,2	0,0
2.1		1354,2	1357,6	0,3
2.2		1354,1	1354,1	0,0
2.3		1354,2	1356,4	0,2
2.4		1267,1	1356,4	7,0
2.5		1201,0	1355,3	12,8
2.6		1201,0	1352,1	12,6
2.7	**a**	1267,0	1298,6	2,5
	b	1267,0	1267,0	0,0
	c	1267,0	1267,0	0,0

6. Discussion

6.1 String of six modules at HIG laboratory

In this chapter it will be discussed the validity of the model designed in LTspice by means of analysing the results submitted in the previous chapter. It is also going to be described how the seven cases of shading proposed affect the performance of the solar array of modules. Additionally, it will be analysed the performance of the three different systems installed at HIG laboratory when they are under the influence of shading.

6.1.1 Validity of the LTspice model

Adjusting the value of the shunt resistance, it has been proved that its value does not have a significant influence on the I-V curve of the module in the group of studied cases. In the Figure 45 it can be seen that for three different R_p values, the I-V curve does not change. Therefore, for the purpose of this master's thesis, it has been considered suitable to use a constant resistance value along the simulations carried out.

To the contrary, the ideality factor has an appreciable effect on the performance of the photovoltaic module. In Figure 45 it can be seen that the curvature of the I-V curve increases when the ideality factor raises its value. It means that the fill factor and the efficiency of the cell decrease with the increment of this factor. On the other hand, the open circuit voltage and the short circuit current are not significantly changed with the change of the ideality factor.

Although it would be better having a smaller value of the ideality factor to have a higher FF value, it depends on the performance of each module and it has to be adjusted with experimental measurements to get the required characteristic values of its cells (I_{SC}, V_{OC}, V_{mp}, I_{mp} and P_{mp}).

The results obtained by the simulations and the ones got by the experimental measurements have been compared in section 5.1 by charts and tables in order to validate the model. From Table 5 to Table 11, the term $|\Delta_{abs}|$ corresponds with the difference between the simulated and the experimental results and the term $|\Delta_{rel}|$ is the percentage of deviation of the simulated results with respect to the experimental data. The maximum relative deviation obtained is 7.1% in case 1.6 (in the maximum power current) followed by 3.5% in case 1.2 (in the cell efficiency deviation). It can be seen that the simulation results obtained with the string layout with bypass configuration model are acceptable, as they mainly agree with the experimental results.

For the case of the 7.1%, it can be observed in Figure 52 that the slope of the curve near the short circuit current does not match the prediction, as the inclination of the curve is higher than it was expected. The reduction of the slope can be a consequence of small mismatches between the short circuit current values of each module. It could be due, for instance, to minor manufacturing variations or different installation angles. If it was the reason, the increment on the slope would also appear in the rest of the

cases, but it is not appreciable in the other simulations so this should not be the reason of this difference. The slope of the I-V curve in this region is also typically affected by the parallel resistance. A reduction in the shunt resistance is responsible of increasing the slope of the I-V curve near the short circuit current and of reducing the FF. This decrement in the shunt resistance may be due to changes within the PV cells or modules. But as it has been tested, the influence of the parallel resistance does not have an important influence in this case study and the decrement in the slope only appears in the last case although the shunt resistance is considered constant for all the cases. The difference in the inclination of the curve could be due to the weather conditions in the moment in which the I-V curve was taken with the I-V tracer, as it was the last case (case 1.6) and some clouds started to appear.

Thus, if this result is not taken into account as it is considered disturbed by weather conditions, the maximum deviation would be 3.5%, which is considered more than acceptable.

In the cases in which the bypass diodes are working, the figures show that the voltage drop in the bypass diodes is too large in the Spice simulations. It can be well appreciated in Figure 51 for instance. The lower step (due to shadow) appears at a smaller voltage in the simulations than in the experimental curves. This fact only affect to the results of case 1.1 as in this case the MPP appears in the higher step, where the bypass diodes are working. However, the effect is small because only one module is shadowed and therefore, only three bypass diodes are working. In the rest of the cases, it does not affect to the results showed in the tables, as the MPP is located in the lower step, in which any bypass diode is working. This problem should be solved adjusting the parameters of the bypass diodes in the electrical model. In this thesis, it has been taken one of the diodes that appears automatically in LTspice library, without changing its parameters and it has been checked that the influence in the simulation results is not important. To have a more accurate model, it would be necessary ask to the module manufacturer for the bypass diodes characteristics and just introduce them into the model as a parameter in a Spice directive.

The I-V tracer takes around 140 different points to draw the I-V curve and the LTspice simulation 250 approximately. If the amount of data tested increased, it would be obtained more accurate results and much of the deviation would be reduced.

Finally, it has to be remarked that the short circuit current and open circuit voltage results perfectly agree with the experimental results, having a maximum relative deviation of 0.25 and 0.86% respectively.

6.1.2 Analysis of the shading effects studied

Once the validation has been done, the equivalent electrical circuit of the string of modules can be used to study any shadow configuration. This makes the model a really useful tool.

In any case, in these paragraphs it will be analysed the seven previous configuration of shadows and how they affect to the performance of the string of modules. In order to be able to compare the different cases, the IV-curve and the maximum power have been simulated for each configuration in STC conditions. These results can be seen in Table 12.

It can be observed that only in the case 1.1 the MPP appears in the high step of the I-V curve. It has almost the same current as in the base case (case 1.0). At this point, through the three bypass diodes of the shaded module is crossing the current difference between the unshaded and the shaded module (as the shaded module generates a current proportional to its unshaded area). So if the unshaded modules generates 5.3 A in this point and the shaded one generates around 3.8 A, the bypass diodes of the shaded cell will conduct 1.5 A. The V_{mp} in this case is 176.96 V, which correspond to the sum of the voltage of the MPP of five modules minus three times the drop in a bypass diode (176.96 V ≃ 214.99/6*5 V-0.7*3 V).

It is very important to correctly design the bypass diodes and how many cells each one covers, because when the bypass diodes are working the cells can suffer irreparable damages, as it has been seen in section 3.6 of the theoretical review. In the string of modules studied, each bypass diode is covering 24 solar cells. So following equation (16), the breakdown voltage of the bypass diodes should be from 12 to 12.5 V to avoid damages in the solar cells. Normally, the diodes have a breakdown voltage of 10 V approximately, so it would be more prudent if each bypass diode covered around 18 to 20 cells.

For the rest of the cases, from 1.2 to 1.6, the MPP is located in the lower step of the curve, which means that all the cells are going to be delivering the same amount of current (3.6 A approximately) and the bypass diodes will not be working. Therefore, in this string system, the delivered power would be almost the same if there were two or more modules with one row shaded.

6.1.3 Performance of the systems installed at HIG laboratory

In these paragraphs it is going to be discussed the performance of the three different systems installed at HIG laboratory when they are under the influence of the seven shading cases analysed above.

Firstly, it has to be said that the power obtained from the DC-DC optimizer system and from the module inverter system should be theoretically the same, as it has been considered that both systems take the maximum power of each of the modules. In these systems, there is not influence of one module to the others, so the effect of shading will be smaller. The power output for both systems would be equal to the sum of the maximum power of the unshaded modules plus the maximum power of the shaded modules. However, this is only theoretically, but in the reality it has to be taken care about the V_{mp} range of the optimizers, because if a module gives a lower voltage than the V_{mp} range of the optimisers or micro inverters systems they will not work. This means that the string inverter will give a higher output.

Analysing Table 12 and Table 13, it can be seen that the power when all the modules are shaded (case 1.6) is the same in the three systems. This is because in the string inverter all the modules are working in their MPP, as there are not steps in the curve and the bypass diodes are not working. The same happens when there are not shadows (case 1.0). Therefore if all the modules have the same shading configuration, there will not be steps in the I-V curve and then both Tigo and Micro inverters will not increase the output.

In the rest of the cases (from 1.1 to 1.5) the output power is greater in the DC-DC optimizer and the module inverter as all the modules are working in their MPP, which is not the case for the bypass system. The difference in the output power reaches its maximum of 18% in the shading case 1.2.

6.2 Effects of shading on the single laboratory module

In this section it will be analysed the effect of different shading configurations in the Windon module. First of all it will be checked that the model is working correctly in this new module using two experimental measurements. After that the different shadow configurations will be analysed. Finally, it will be studied the performance of six modules connected in series, five unshaded and one shaded, comparing their performance in case of having only bypass diodes or also DC-DC optimizers.

6.2.1 Validation of the model and adjustment of the ideality factor

The results show a good agreement between experimental and simulation results as it can be seen in Figure 54 and Figure 55, with a maximum relative deviation of 2.8%. Therefore, the model of the Windon module is also validated and it can be used to simulate the rest of cases.

Additionally, the adjustment of n and R_p carried on shows that just as in the string of modules discussed in section 6.1 the value of the shunt resistance does not have a significant influence, while the value of the ideality factor that better fits the experimental measurements is n=1.8. These conclusions have been taken from Figure 53.

6.2.2 Analysis of the shading effects studied

To begin with, comparing the case 2.1 in which one cell is 50% shaded with the base case (without shading), it can be observed that as a consequence of the shadowing it appears a step approximately at 22.5 V, which corresponds to the voltage of the two circuits of the module which are not shaded. Therefore, if the voltage in the module is lower than 22.5 V, the bypass diode of the third circuit will be working to conduct the difference of current that the shaded circuit cannot generate (9.4-4.7≃4.7 A). On the other hand, if the voltage is higher than 22.5 V none of the three bypass diodes will be working as the three circuit will generate the same current (4.7 A). In this case, it can be seen in Figure 54 that the MPP appears in the lower step, so the diodes will not be working. The effect of having one cell shaded is the reduction of the maximum power from 240.2 to 156.5 W.

Secondly, it can be seen that if the percentage of the shaded area increase the lower step of the I-V curve decrease, as the current in the shaded circuit will be lower. It can be analysed comparing Figure 57 and Figure 58. In this case, the MPP appears in the higher step, with a value of 153 V. The bypass diode of the shaded circuit will be working in this case. The maximum power has not decreased a lot with respect case 2.1 because the higher step (corresponding to the two unshaded circuit) is the same in both cases, and in case 2.1 the two peaks of power are similar. So it can be concluded that in this module, if there is only one cell shaded, the maximum power obtained will

be very similar when the shaded area is higher than 50% of the cell, regardless the percentage of shadowing.

In addition, it has been proved that if there are more than one cell in the same circuit that are shaded the same area, as in case 2.3 compared with case 2.1, the performance will be the same independently of the number of cell shaded. Therefore, the curves in Figure 57 and Figure 59 are the same. This is because although there was only one cell shaded, the current of this bypass circuit would already be restricted to the maximum that the shaded cell can generate. This would be also the case of having one column with a constant percentage of shadow, which is a shadow configuration that sometimes appears in the roof modules. The performance will be the same than if there were only one cell shaded with the same fraction.

On the contrary, if the shaded cells correspond to different bypass circuits, as in case 2.4 with respect 2.3, the curves will change, as the higher step appears at 11 V approximately. This voltage corresponds to the voltage of the unshaded circuit. This performance can be seen in Figure 60. The MPP is almost the same as in 2.3 and 2.1 because the power in the lower step is identical.

When all the bypass circuits have the same shadow configuration, there will only be one step in the I-V curve, as all the circuits will generate the same current and the bypass diodes will not be working. That happens in cases 2.5 and 2.6, which have the same performance because it does not matter how many cells are shaded in the same circuit if they have the same percentage of shading. It can be observed in Figure 61 and Figure 62. The power in both cases is similar to the power in the previous cases 2.1, 2.3 and 2.4 as the MPP is also in the lower step.

To conclude the different shading configurations, it has been shown that when each bypass circuit has a different percentage of shading, it appears three different steps, as in case 7 (Figure 63). In this case it has been tested the three shadowing percentages summarised in Table 4. In this figure, it can be observed that the higher step of the I-V curve is the same in the three configurations, as in all of them the third bypass circuit is not shaded. On the contrary, in the lower and the middle steps, it can be seen that when there is less shadowed area (as in the case of 70% and 58% of shadowing), the current in these steps is higher and so the power is higher. It is interesting to remark that there is a configuration of shadowing in which the three peaks of power have the same maximum power. In this module it occurs in case 2.7.b, for 80%, 68% and 0% of shadowing in each bypass circuit respectively. It is represented by the green line of Figure 63.

6.2.3 Performance of optimizer systems with shadows

As a final point, it will be studied the benefits of installing optimizers in each module by means of comparing the performance of a string of six modules in series with one module shaded. As it has been explained, the optimizer gives the maximum power of each of the modules.

It will be analysed what happens when there is not optimizer. If there are six modules in series with only one of the modules shaded, the current of the MPP of the string will be the one generated in the unshaded modules (around 8 A in this case), and the operation point of the shaded module will be determined by this current. Therefore,

when the MPP of the shaded module appears at this current (in the high step corresponding to an unshaded bypass circuit), the maximum power of the string will be almost the same with or without optimizer, as all the modules will be working in their MPP. Analysing Table 18 it can be seen that this fact occurs in case 2.2 in which the shaded area is 75%. Cases 2.1 and 2.3 have also almost the same performance, as the two MPP of the shaded module are really similar. Accordingly, it can be conclude that if the shadow in one bypass circuit is higher than 50%, the performance will be the same with or without optimizer.

On the contrary, when the module has more than one bypass circuit shaded, as in case 2.4, the power will be much lower without optimizer as the shaded module will be working in the higher step and the MPP of the module occurs in the lower step. The increment of power using optimizer in this case will be almost 90 W.

In the cases 2.5 and 2.6, as all the bypass circuits of the shaded module are suffering shadowing, the three bypass diodes will be working and the shaded module will not give any power in the case without optimizer. Consequently, the increment of power with the usage of optimizer will be really high, more than 150 W, as it can be seen in Table 18.

To conclude with, in case 2.7 can be seen that if the shadows in the circuits are largar than the value which makes the three peaks equal, the optimizer does not increase the output power. This is because the MPP is in the higher step, at a current similar to the operating point of the string. This happens in cases 2.7.b and c. On the other hand, if the percentage of shading is lower, the output power will increase with the use of the optimizer.

7. Conclusions

Firstly the validation of the models has been performed:

- PV systems modelling and simulation in LTspice environment have been presented and validated by means of a comparative analysis with the experimental results obtained in a set of tests carried out in the laboratory of Gävle University.

- The simulation results show a remarkable agreement with the experimental data, which means that the model designed at LTspice supposes a very useful tool that can be used to study the performance of PV systems.

In addition, the effect of different shading configurations has been analysed:

- In the first group of cases studied (string of six modules at HIG) the results show that the output power will be almost the same if there are two or more modules shaded in the string. If there is only one shaded module, the output will be higher.

- It has been shown that in order to avoid damages in solar cell, it would be more reasonable to reduce the amount of cells that each bypass diode covers from 24 to 20 cells.

- In the Windon module research, the in-depth analysis of the impact of shading carried out facilitates the understanding of the performance of PV modules under different shadowing effects.

Finally, it has been seen the benefits of installing a DC-DC optimizer or a module inverter:

- An optimizer increases the power from a shaded series connected module if all three circuits in the module are shaded.

- In the case of the string of six modules, it has been seen that installing an optimizer will not increase the output when all six the modules have the same shadowing configuration or are unshaded.

- On the other hand, in the research made to the single module at the laboratory, it is concluded that it is beneficial to install an optimizer when the module has one bypass circuit shaded less than 50% or two bypass circuits shadowed less than 80%, which means that the MPP of the module is in the lower step of the I-V curve.

- The installation of optimizers does not always increase the performance. Therefore, before installing them, it is necessary to study the shadowing configurations that the system suffers.

References

[1] S. H. Kim, C. M. Cracken and J. Edmonds, “Solar Energy Technologies and Stabilizing Atmospheric CO2 Concentrations”, *Progress in photovoltaics: research and applications,* vol. 2000, no. 8, pp. 3-15, 2000.

[2] M. S. Cengiz and M. S. Mamiç, “Price-Efficiency Relationship for Photovoltaic Systems on a Global Basis”, *International Journal of Photoenergy,* vol. 2015, no. 256101, pp. 1-12, 2015.

[3] R. Ramakumar and J. E. Bigger, “Photovoltaic Systems”, *IEEE Journals & Magazines,* vol. 81, no. 3, pp. 365-377, 1993.

[4] Union of Concerned Scientists, “How Solar Panels Work”, December 2015. [Online]. Available: http://www.ucsusa.org/clean-energy/renewable-energy/how-solar-panels-work#.VyjSvvmyOko. [Accessed May 2016].

[5] Samlex Solar, “Solar (PV) Cell, Module, Array”, 2014. [Online]. Available: http://www.samlexsolar.com/learning-center/solar-cell-module-array.aspx. [Accessed May 2016].

[6] S. R. Wenham, M. A. Green, M. E. Watt, R. Corkidh and A. Sproul, Applied photovoltaics, third edition, ISBN 978-1-84977-698-1, Abingdon, Oxon: Earthscan, 2012.

[7] G. Conibeer, “Third-generation photovoltaics”, *Materials today,* vol. 10, no. 11, pp. 1-9, 2007.

[8] S.K. Nashih et al., “Numerical Approach to the Analysis of Shading Effects on Photovoltaic Panels”, Gävle, Sweden, March 2015

[9] M. Azzouzi, “Modeling and simulation of a photovoltaic cell considering single-diode model”, *Recent Advances in Environmental Science and Biomedicine ,* pp. 175-182, Ziane Achour University of Djelfa, Algeria, 2014.

[10] S. Silvestre and A. Chouder, “Effects of Shadowing on Photovoltaic Module Performance”, P*rogress in photovoltaics: research and applications,* vol. 2008, no. 16, pp. 141-149, 2008.

[11] V. Tamrakar, S. C. Gupta and Y. Sawle, “Single-diode and Two-diode PV cell modelling using Matlab for studying characteristics of solar cell under varying conditions”, *Electrical & Computer Engineering: An International Journal (ECIJ),* vol. 4, no. 2, pp. 67-77, 2015.

[12] S. Chandra, J. Kumar, S. K. Udgata and V. Bhateja, Information System Design and Intelligent Applications, ISBN 978-81-322-2756-4, Nadia, India: Springer, 2016.

[13] M. C. Alonso-García and J. M. Ruíz, "Analysis and modelling the reverse characteristic of photovoltaic cells", *Solar Energy Materials & Solar Cells,* vol. 2006, no. 90, pp. 1105-1120, 2006.

[14] Solmetric, "Guide To Interpreting I-V Curve Measurements of PV Arrays", 1 March 2011. [Online]. Available: http://www.solmetric.com/newsletters.html. [Accessed 28 April 2016].

[15] M. Tivanov, A. Patryn, N. Drozdov, A. Fedotov and A. Mazanik, "Determination of solar cell parameters from its current-voltage and spectral characteristics", *Solar Energy Materials & Solar Cells,* vol. 2005, no. 87, pp. 457-465, 2005.

[16] A. Vossier, F. Gualdi, A. Dollet, R. Ares and V. Aimez, "Approaching the Shockley-Queisser limit: General assessment of the main limiting mechanisms in photovoltaic cells", *Journal of applied physics,* vol. 2015, no. 117, pp. 015102 1-8, 2015.

[17] Q. A. Al-Naser, N. M. Al-barghoothi and N. A. Al-Ali, "The Effect of Temperature Variations on Solar Cell Efficiency", *International Journal of Engineering, Business and Enterprise Applications (IJEBEA),* vol. 2013, no. 13, pp. 108-112, 2013.

[18] A. El-Shaer, M. T. Tadros and M. A. Khalifa, "Effect of Light intensity and Temperature on Crystalline Silicon Solar Modules Parameters", *International Journal of Emerging Technology and Advanced Engineering,* vol. 4, no. 8, pp. 311-318, 2014.

[19] J.F. Contero, "Shadowing Effect on the Performance in Solar PV-Cells", Master's thesis, Building, Energy and Environmental Engineering department, University of Gävle, Sweden, June 2015

[20] A. Woyte, J. Nijs and R. Belmans, "Partial shadowing of photovoltaic arrays with different system configurations: Literature review and field test results", *Solar Energy,* vol. 3, no. 74, pp. 217-233, 2003.

[21] P. C. Bronsveld, G. Coletti, P. Barton, P. Manshanden and L. J. Geerligs, "Differences in reverse bias voltage behavior of n-type and p-type multicrystalline solar cells", *Energy Procedia,* vol. 27, no. 2012, pp. 109-115, 2012.

[22] M. Barbato, A. Barbato, M. Meneguini, A. Cester, G. Mura, D. Tonini, A. Voltan, G. Cellere and G. Meneguesso, "Reverse bias degradation of metal wrap through silicon solar cells", *Solar Energy Materials and Solar Cells,* vol. 147, no. 2016, pp. 288-294, 2016.

[23] H. Yang, H. Wang and M. Wang, "Investigation of the Relationship between Reverse Current of Crystalline Silicon Solar Cells and Conduction of Bypass Diode," *International Journal of Photoenergy,* vol. 2012, no. 357218, pp. 1-5, 2012.

[24] Linear Technology, “Design Simulation and Device Models,” [Online]. Available: http://www.linear.com/designtools/software/. [Accessed 24 April 2016].

[25] Y. Khalaf, O. Ibraheem, M. Adil, S. Mohammed, M. Qasim and K. Waleed, “Maximum power point evaluation of photovoltaic modules under shading effect”, *European Scientific Journal,* vol. 10, no. 9, pp. 281-294, 2014.

Appendix

1. EuroLink PRO programme curves

In this appendix are included the curves from Figure 65 to Figure 73, obtained in the experimental tests carried out at HIG laboratory and downloaded using EuroLink PRO. This data has been used in the thesis to compare and validate the simulation results obtained from the LTspice models.

1.1 String of six modules at HIG laboratory

- Case 1.0: not shading in the modules, base case:

Figure 65: EuroLink PRO curves for case 1.0

- Case 1.1: 37% of a row shaded in one module:

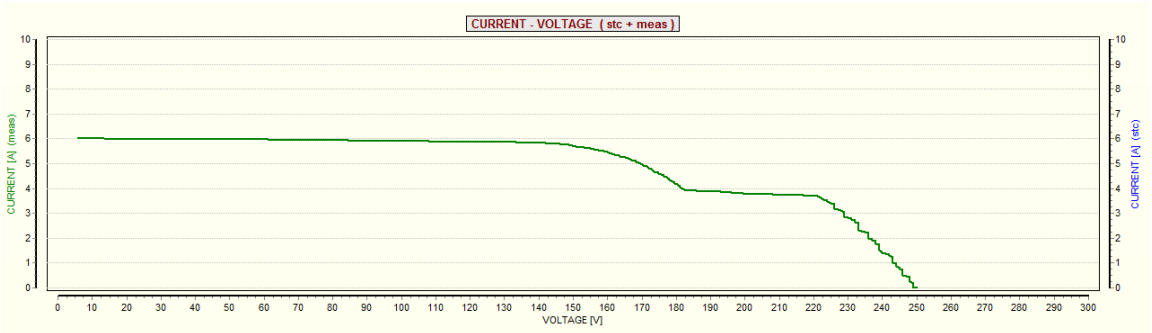

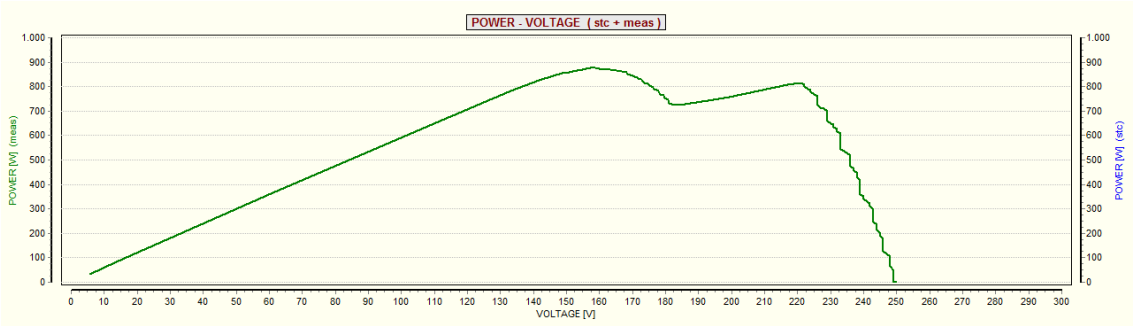

Figure 66: EuroLink PRO curves for case 1.1

- Case 1.2: 37% of a row shaded in two modules:

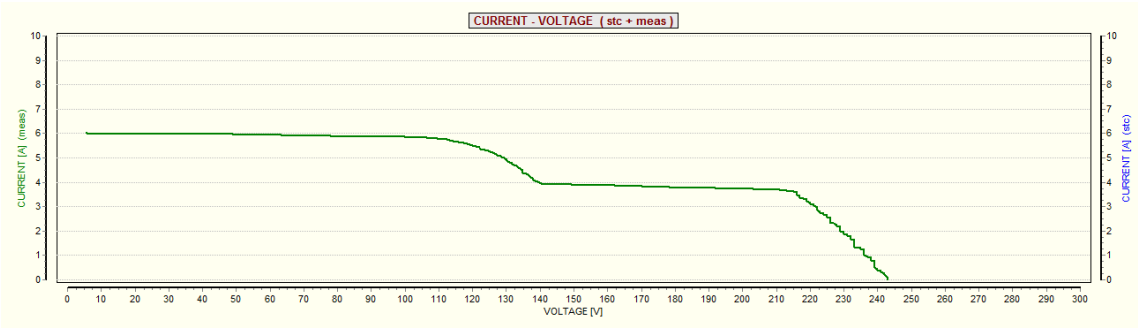

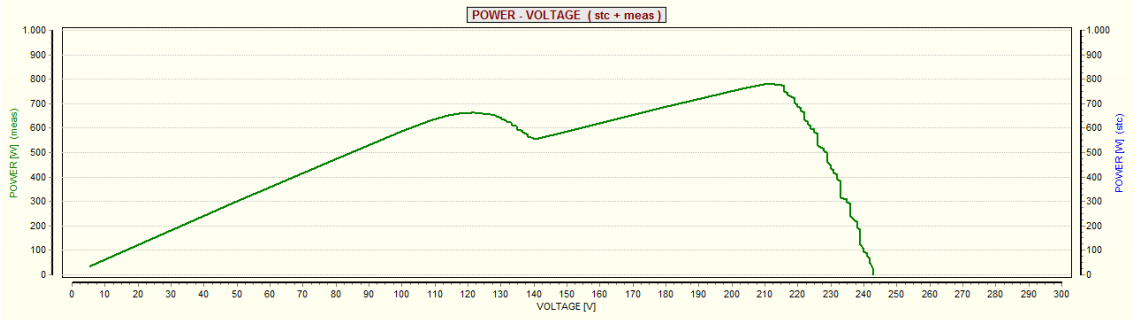

Figure 67: EuroLink PRO curves for case 1.2

- Case 1.3: 37% of a row shaded in three modules:

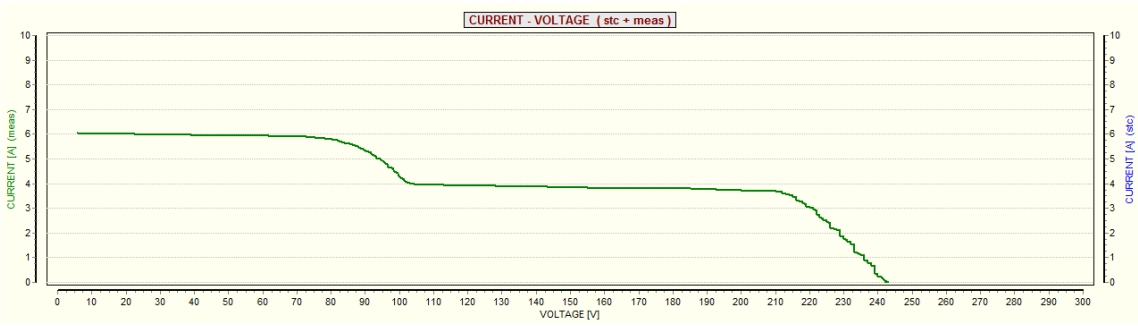

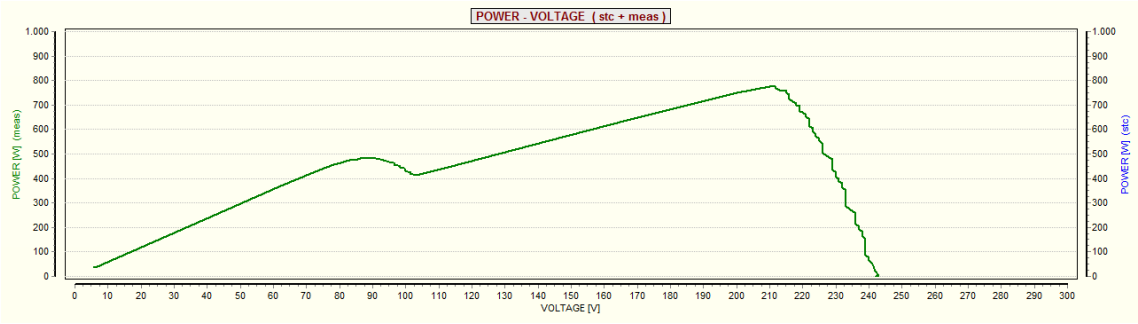

Figure 68: EuroLink PRO curves for case 1.3

- Case 1.4: 37% of a row shaded in four modules:

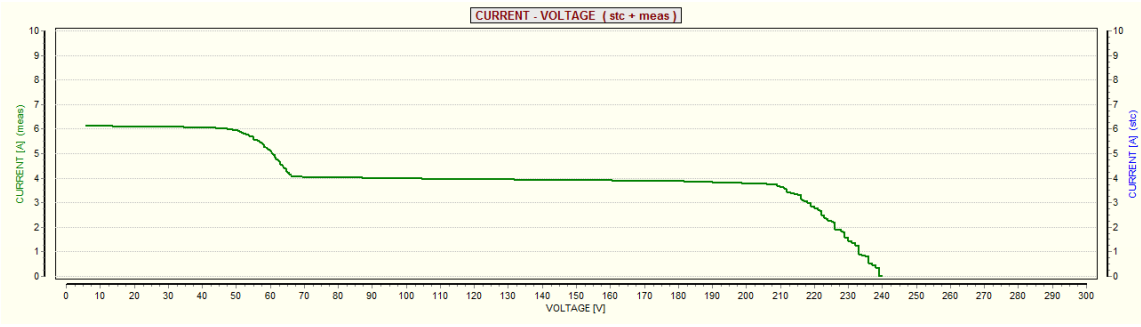

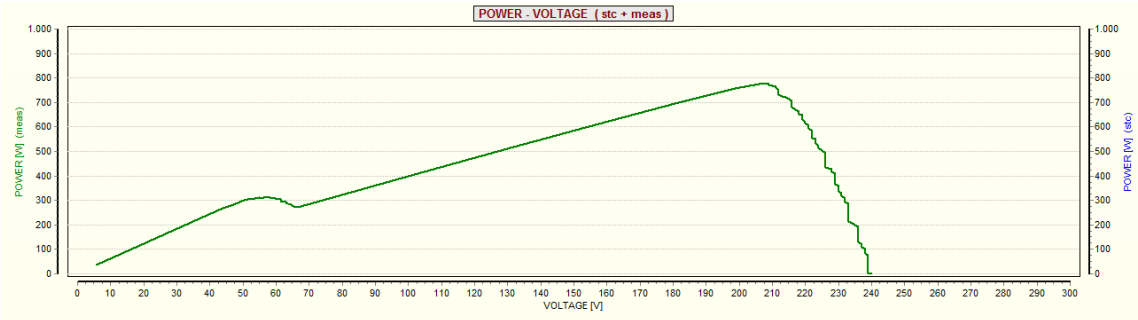

Figure 69: EuroLink PRO curves for case 1.4

- Case 1.5: 37% of a row shaded in five modules:

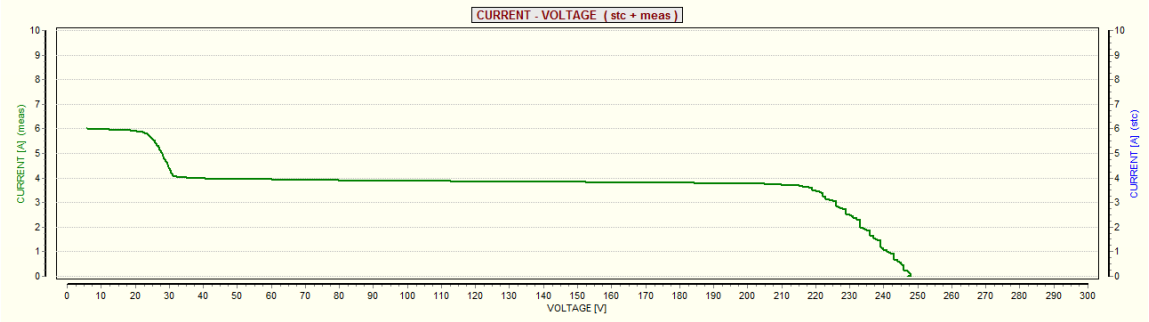

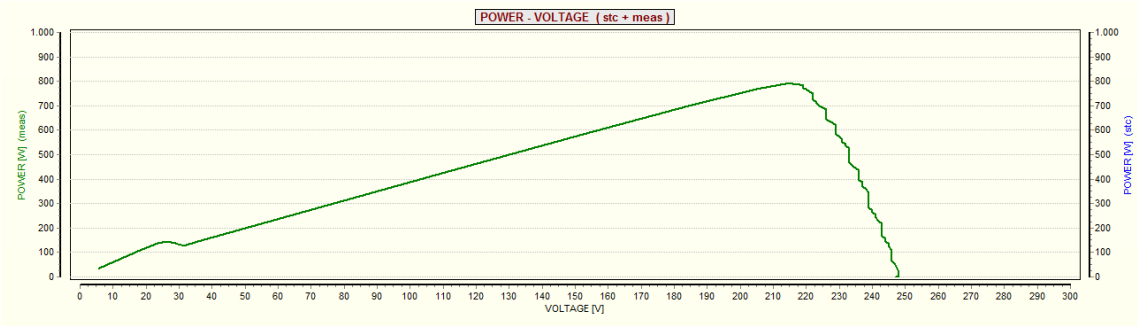

Figure 70: EuroLink PRO curves for case 1.5

- Case 1.6: 37% of a row shaded in six modules:

Figure 71: EuroLink PRO curves for case 1.6

1.2 Effects of shading in the laboratory module

- Case 2.0: not shading in the module, base case:

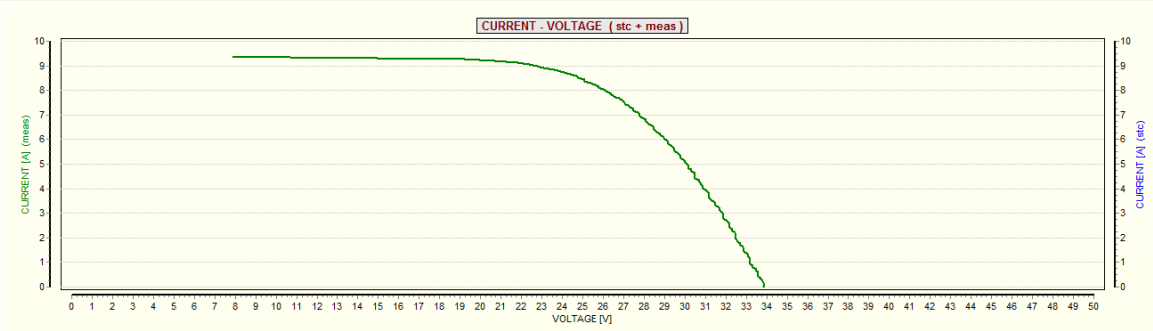

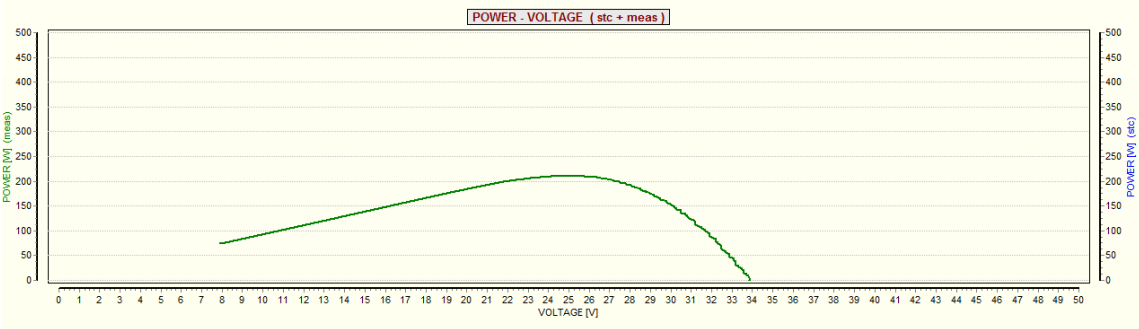

Figure 72: EuroLink PRO curves for case 2.0

- Case 2.1: 50% of a cell shaded:

Figure 73: EuroLink PRO curves for case 2.1